Ref. Ares(2026)1118084 - 31/01/2026

Secured and Intelligent Massive Machine-to-Machine Communications for 6G (SCION)

D5.1: Digital Twin modeling for M2M use cases

Version: v2.0

Document type	Report
Dissemination level	P (Public)
Lead editor	KTH
Contributors	Yingzhuo Sun, Ming Xiao
Work package	WP5 (Task 5.1)
Keywords	Digital Twin, M-LEO, multi-orbit satellite selection, matching game theory, resource allocation.

ABSTRACT

Multi-orbit low-Earth-orbit (M-LEO) constellations are a key enabler for space–air–ground integrated networks (SAGINs), but their fast time-varying visibility and heterogeneous resources make joint user association and resource allocation challenging. This technical report consolidates our recent research results into an implementation-oriented description. We formulate a dynamic mixed-integer optimization problem that couples satellite/sector selection with user association, bandwidth allocation and power allocation, and we present a practical two-level solution that combines a Markov-approximation outer search with a matching-game and Lagrangian-dual inner optimizer. Simulation results (with STK-generated satellite trajectories) demonstrate the convergence behaviour and performance advantages compared with representative baselines under QoS constraints. The results demonstrate that the proposed algorithm outperforms the best-performing baseline, achieving an average improvement of approximately 7.85% in sum-rate.

Funding and Disclaimer





Funded by the European Union's Horizon Europe programme under the Marie Skłodowska-Curie Actions Doctoral Networks Grant Agreement No. 101072375. Views and opinions expressed are however those of the author(s) only and do not necessarily reflect those of the European Union. Neither the European Union nor the granting authority can be held responsible for them. The UK institutions were funded by UK Research and Innovation (UKRI) under the UK government's Horizon Europe funding guarantee [grant numbers EP/X027201/1 and EP/X027244/1.]

Document revision history

Date	Author (partner's name)	Contribution
15.01.2026	Yingzhuo Sun (KTH), Ming Xiao (KTH)	v1.0: First version
16.01.2026	S. Mumtaz (NTU)	First Review
26.01.2026	Yingzhuo Sun (KTH), Ming Xiao (KTH)	V1.1 Revision
27.01.2026	S. Mumtaz (NTU)	Second Review
29.01.2026	B. Özbek (IYTE)	Final Editing
30.01.2026	Yingzhuo Sun (KTH), Ming Xiao (KTH)	V2.0: Final Version

©2023-2027 SCION Consortium. All rights reserved.

Table of Contents

Executive Summary **1**

1 Introduction **2**
1.1 Motivation of M-LEO in SAGINS . . . 2
1.2 Digital Twin in Satellite Communication . . . 2
1.3 Brief Summary of Satellite Constellation Design . . . 2
1.4 Proposed Framework in the report . . . 3

2 Related work **5**
2.1 M-LEO Satellites Selection . . . 5
2.2 Digital Twin in Satellites Network . . . 6

3 System Model and Problem Formulation **8**
3.1 Network Model . . . 8
3.2 Zenith Angle Rule . . . 8
3.3 Transmission Model . . . 9
3.4 Problem Formulation . . . 11

4 The Proposed DV-MOS2 Framework **13**
4.1 Markov Approximation . . . 13
4.2 Matching Game Theory . . . 16
4.2.1 User Association . . . 17
4.2.2 Bandwidth Allocation . . . 20
4.3 Lagrangian Dual-Based Optimization for PA . . . 20
4.4 Algorithm Summary . . . 23

5 Simulation Results **24**
5.1 Simulation Environments and Settings . . . 24
5.2 DV-MOS2 Approach Verification . . . 24
5.2.1 DV-MOS2 Convergence Verification . . . 24
5.2.2 Behavior of Matching Game-based UA and BA in DV-MOS2 . . . 24
5.2.3 Effectiveness of JUBPA in DV-MOS2 . . . 25
5.3 Performance Comparison . . . 26
5.3.1 Gains of Joint UA-BA Matching in DV-MOS2 . . . 26
5.3.2 Comparative evaluation of Satellite Selection Strategies under Dynamic Visibility . . . 27
5.3.3 Sensitivity analysis . . . 29

6 Conclusion and Future Work **30**

7 Appendix **31**
7.1 Proof of Theorem 1 . . . 31
7.2 Proof of Theorem 2 . . . 31

©2023-2027 SCION Consortium. All rights reserved.

List of Figures

1 M-LEO satellite communication network. 9
2 DT-assisted satellites communication network. 9
3 Illustration of the zenith angle rule. 11
4 Overall workflow of the proposed DV-MOS2 framework. 14
5 Spatial distributions of (a) satellites with UE and (b) UE. 25
6 DV-MOS2's sum rate (a) convergence and (b) CDF curve under different setup of SF values. 26
7 Convergence of matching game process under different network sizes. 26
8 Convergence of JUBPA algorithm under different setup of SF values. 26
9 Sum rate comparison of different matching algorithms and different angle values. 27
10 Sum rate comparison of different satellites selection algorithms. 27
11 Visualized satellite trajectories: (a) 2D at $t = 1$, (b) 3D at $t = 1$, (c) 2D at $t = 7$, (d) 3D at $t = 7$, (e) 2D at $t = 9$, (f) 3D at $t = 9$, (g) 2D at $t = 15$, (h) 3D at $t = 15$. 28

©2023-2027 SCION Consortium. All rights reserved.

Abbreviations

BA	Bandwidth Allocation
BS	Base station
DT	Digital Twin
DV-MOS2	Dynamic visibility-aware multi-orbit satellite selection framework
GEO	Geostationary Earth Orbit
JUBPA	Joint UA,BA and PA Algorithm
KKT	Karush-Kuhn-Tucker
LEO	Low Earth Orbit
M-LEO	Multi-orbit LEO constellation
M2M	Machine to machine
PA	Power Allocation
PE	Physical entity
QoS	Quality of Service
RA	Resource Allocation
SAGINs	Space–Air–Ground Integrated Networks
STK	Systems Tool Kit
UA	User Association
UE	User equipment
VE	Virtual entity

©2023-2027 SCION Consortium. All rights reserved.

Executive Summary

This report provides the first deliverable of WP5, Task T5.1 “Digital Twin modeling for M2M use cases”, and presents a DT-based modelling approach to enable intelligent decision-making in complex, high-performance machine-to-machine (M2M) communication systems. The deliverable is written to support practical integration into the SCION framework, with particular emphasis on two themes: DT-enabled representation of M2M systems and satellite-assisted connectivity as a time-varying, resource-constrained communication substrate.

The document begins by establishing the DT modeling foundations required for M2M operation. In line with the DT concept, the whole system is represented by a physical communication system, a physical entity (PE) and a corresponding virtual entity (VE) which is the proposed algorithm used to make the decision. The report provides a structured basis for monitoring, prediction, and closed-loop decision making in dynamic M2M deployments. A simple closed-loop example is as follows: at the beginning of a slot, the PE reports the current visible-satellite set from coordinates, per-satellite power budgets, and the achieved/required rates of active M2M flows. The VE then runs the proposed visibility-aware selection and allocation algorithm to choose which satellites are activated and to compute the corresponding user association and bandwidth/power allocation for this slot. These decisions are pushed back to the PE for actuation, and the resulting performance indicators are fed back to the VE to update the next-slot decision.

Based on the basic elements, the report then focuses on how satellite networks can be embedded into the DT as a typical DT M2M communication scenario. Since LEO satellite visibility, beam coverage, and interference conditions vary rapidly over time, the DT must incorporate time-indexed network states and constraints that influence end-to-end service delivery. To this end, the document adopts a visibility-aware satellite network model and formulates a slot-wise optimization problem that jointly determines which satellites are activated, how M2M endpoints are associated to satellites and sectors, and how bandwidth and power are allocated under per-satellite budgets and minimum-rate QoS constraints.

A key contribution of this deliverable is a tractable DT-driven decision workflow that couples discrete satellite-set adaptation with resource allocation, enabling the DT to support actionable network control rather than passive monitoring. The proposed solution combines an outer, Markov-approximation-based mechanism that explores satellite-selection states while favoring high-utility configurations, with an inner optimization routine that stabilizes association and bandwidth decisions and computes feasible power allocation via dual-based updates. The report retains the full modeling and algorithmic details and supports the methodology with numerical studies based on realistic satellite trajectories, demonstrating how DT-aware satellite selection and resource allocation can improve service performance under time-varying connectivity.

Finally, the report identifies practical challenges and next steps for WP5 as DT modelling is extended toward system-level deployment. These include maintaining timely and scalable VE/PE/CN synchronisation under fast LEO dynamics, incorporating additional service constraints relevant to M2M use cases , and bridging DT outputs to implementable control actions in real-time network management. The document also outlines directions for integrating the proposed DT modelling and satellite-assisted optimisation workflow into broader SCION use cases, where satellite connectivity, terrestrial infrastructure, and edge intelligence must be orchestrated in a unified DT-enabled closed loop.

©2023-2027 SCION Consortium. All rights reserved.

1 Introduction

In recent years, with the ever-growing demand for higher data rates and ubiquitous connectivity, terrestrial fifth generation (5G) networks are increasingly unable to satisfy the requirements of future communication services [1]. While the sixth generation (6G) vision emphasizes global coverage as one of its key targets [2], existing terrestrial infrastructures remain constrained by geography, leaving users in remote, rural, and maritime areas underserved due to the lack of base station deployment [3]. To overcome these limitations, multi-orbit low-earth-orbit (M-LEO) satellite systems are envisioned as an infrastructure to provide seamless connectivity with truly global coverage, bridging underserved regions and enhancing the resilience of space-air-ground integrated networks (SAGINs) [4].

1.1 Motivation of M-LEO in SAGINS

M-LEO systems' primary advantages include low launch cost enabled by mature commercial rocket technology, and low round-trip communication delay owing to the relatively short propagation distance. However, deploying large-scale M-LEO constellations inevitably introduces significant network complexity due to the massive number of satellites and high velocity. In particular, the resulting highly dynamic constellation leads to a time-varying set of visible satellites over any given region, making adaptive satellite selection essential for ensuring reliable connectivity to user equipment (UE) within the service area.

1.2 Digital Twin in Satellite Communication

To deal with the challenge brought by the high complexity of M-LEO network and requirements of selecting satellites adaptively, Digital Twin (DT) can be introduced. The concept of DT has been proposed to supply real-time data transmission and simulations through applying the bidirectional data exchange between the digital replica and physical twin. DT was conducted to design the spacecrafts and to improve the products quality in the first place. As DT becomes more developed and mature, it has been widely used to design aerospace products and assemble manufacturing. Recently, it is also introduced into the area of network simulation and satellite modeling because the system performance can be evaluated in a more cost-effective way.

1.3 Brief Summary of Satellite Constellation Design

Existing research efforts have been devoted to addressing the challenges of satellite constellation design, user association (UA), and resource allocation (RA). Among the early contributions in this area, [5] developed a three-dimensional constellation design algorithm to minimize the number of satellites while ensuring backhaul requirements. Another vast corpus of literature has focused on UA and RA under fixed constellation settings. For instance, [6] formulated the UA problem between ground UEs and LEO satellites, but the study assumed only three fixed satellites and did not consider satellite selection. Beyond fixed settings, several studies investigated satellite selection strategies. A single-satellite selection problem was modeled in [7], where remaining service time, access times, and storage capacity were adopted as metrics, and a genetic algorithm was used for optimization. Multi-satellite selection was explored in [8]. A joint beamforming and UA design was proposed but the dynamic variation of visible satellites was not considered. To capture long-term selection dynamics, [9]

©2023-2027 SCION Consortium. All rights reserved.

introduced a non-dominated sorting optimization algorithm for M-LEO selection in global navigation satellite systems, considering signal strength, and residual visibility time.

Despite these advances, most existing studies as aforementioned are conducted under fixed constellation assumptions, where the set of serving satellites is predetermined and static. These common assumptions may be reasonable for simplified scenarios with a small number of satellites, but they become unrealistic in large-scale M-LEO systems. In practice, satellites in different orbital planes and with varying relative phases move continuously, leading to a dynamic and time-varying set of visible satellites over any specific region. This dynamic visibility introduces two critical challenges. 1) the number of visible satellites fluctuates significantly over time, ranging from dense situations with many candidate satellites to sparse conditions with only a few feasible connections; 2) even when multiple satellites are simultaneously visible, their link qualities vary due to differences in elevation angles, residual visibility time, and interference conditions. These factors imply that both the number of satellites to be selected and the identity of the serving satellites must be adapted dynamically, rather than being fixed in advance.

1.4 Proposed Framework in the report

To bridge these important gaps, we put forward the dynamic visibility-aware multi-orbit satellite selection framework (DV-MOS2), which integrates constellation-level satellite number adaptation with fine-grained per-satellite selection across multiple orbital layers. In particular, we investigate a scenario where UE in the service area may be simultaneously covered by multiple candidate satellites, and the network controller must dynamically determine the optimal number of serving satellites, the satellite-UE associations, and the transmit power allocation. The objective is to maximize the UE sum-rate under per-satellite power budget constraints and overall constellation size limitations. Notably, the number of visible M-LEO satellites varies significantly across time slots. This dynamic visibility makes the problem more challenging, as it results in a time-varying feasible set of candidate satellites, enlarges the combinatorial search space, and tightly couples the decisions of satellite selection, UA, and power allocation (PA) under constellation size constraints. The main innovations and contributions of this report can be summarized as follows.

- For the first time, we investigate the sum-rate maximization problem through the joint design of multi-orbit satellite selection, association control, and PA under constellation size constraints in a M-LEO setting. A key novelty is that, instead of assuming a fixed set of serving satellites, our problem setting explicitly models the temporal evolution of candidate satellite sets. Incorporating dynamic visibility together with constellation size constraints changes the problem setting drastically and takes us beyond conventional M-LEO frameworks, since satellites in different orbital planes and with varying relative phases continuously enter and exit the cone-shaped visibility regions of ground UEs, making the feasible set inherently time-varying. Consequently, the formulated problem is rendered NP-hard by the joint impact of dynamic visibility and constellation size limitations because it is a mixed-integer non-convex optimization problem.
- To address the above challenges, we propose DV-MOS2 combining Markov approximation and matching game theory. Specifically, we design an ergodic Markov chain with tailored transition probabilities that guarantee convergence to its stationary distribution. Built upon this reformulation, we further develop a two-phase algorithm, where matching game theory determines stable satellite-UE associations and Lagrangian dual-based

©2023-2027 SCION Consortium. All rights reserved.

optimization for PA. This integrated approach achieves near-optimal performance with guaranteed convergence and significantly lower complexity than heuristic alternatives.

- We conduct extensive experiments on the Walker Constellation Design Pattern To gain insight into the proposed DV-MOS2, we provide a comparative analysis against four state-or-the-art benchmark methods. The results demonstrate that DV-MOS2 consistently outperforms the best-performing baseline, achieving an average improvement of approximately 7.85% in sum-rate.

The report is organized as follows. Section 2 reviews the related work, covering both M-LEO satellite selection/UA/RA studies and recent progress on digital-twin-enabled satellite networks. Section 3 introduces the system model and problem formulation, including the network model, the zenith-angle-based dynamic visibility rule, the transmission model, and the resulting joint optimization problem. Section 4 presents the proposed DV-MOS2 framework, detailing the Markov-approximation outer search and the inner JUBPA procedure composed of matching-game-based UA/BA and Lagrangian-dual power allocation, together with a summary of algorithmic properties. Section 5 reports simulation settings and numerical results, including convergence verification and performance comparisons against representative baselines. Finally, Section 6 concludes the report and outlines future work directions.

©2023-2027 SCION Consortium. All rights reserved.

2 Related work

2.1 M-LEO Satellites Selection

Research on M-LEO satellite communication and RA in SAGINs has gained significant attention in recent years. Prior studies provide valuable insights into constellation design, UA/RA, and satellite selection strategies, yet many rely on simplified assumptions (e.g., fixed constellations or decoupled UA and RA) that limit applicability in large-scale, dynamic M-LEO systems. To position our work, we group the literature into four categories: fixed-constellation UA/RA, single-satellite selection, static multi-satellite/multi-orbit selection, and long-term multi-satellite selection. A condensed comparison of common assumptions and limitations is provided in Table 1.

1) Optimization under Fixed Constellations: A common paradigm assumes a fixed LEO constellation and optimizes UA/RA under snapshot-like network states. For example, [10] uses stochastic geometry to analyze nearest-satellite versus max-SINR access and derives closed-form metrics such as coverage probability and non-handover probability, while [11] employs deep reinforcement learning to improve resource utilization under uneven traffic demands. More representative works and their shared assumptions/limitations are summarized in Table 1.

2) Single-Satellite Selection Approaches: Some studies restrict each UE to a single serving LEO satellite to simplify association decisions. In [12], the selection is formulated as a potential game where satellites and frequency bands are treated as shared resources among competing UEs, leading to distributed association decisions; [7] further integrates a random-access mechanism within an SDN framework to improve area sum-rate under this one-satellite constraint. See Table 1 for a compact view of this line of work.

3) Multi-Satellite or Multi-Orbit Selection Methods: Beyond single-satellite settings, static (or snapshot-based) multi-satellite selection has been explored using optimization and matching tools. For instance, [13] applies user-division matching together with the Gale–Shapley method to maximize downlink sum-rate, whereas [14] combines ADMM and convex-optimization routines to jointly handle satellite selection and access with objectives such as sum-rate, fairness, and energy efficiency. A brief category-level comparison is given in Table 1.

4) Long-Term Multi-Satellite Selection: Long-term strategies explicitly account for temporal evolution of satellite availability and are often motivated by handover stability. For example, [25] designs a conditional handover optimization based on service continuity graphs to predict handover sequences and reduce handover rates, while [30] formulates long-term beam management and resource decisions via Lyapunov-based decomposition under dynamic conditions. Table 1 summarizes the two sub-lines (with and without explicit UA/RA) and their common limitations.

Across the above categories, three recurring gaps remain. First, dynamic satellite-set adaptation driven by fast time-varying visibility (especially in multi-orbit M-LEO systems) is often simplified or missing. Second, when satellite selection is coupled with UA/RA, per-slot feasibility under minimum-rate QoS and per-satellite power budgets is not consistently guaranteed. Third, scalability for slot-level control in large constellations remains challenging due to optimization or training overhead. These gaps motivate the dynamic visibility-aware satellite selection and tractable joint UA/BA/PA workflow developed in this report.

©2023-2027 SCION Consortium. All rights reserved.

Table 1: Related-work of LEO satellite UA/RA and satellite selection.

Category	Key works	Assumptions	Limitations
Fixed-constellation	[6, 10, 11, 15–18]	Fixed satellite set; snapshot; simplified interference/CSI	No set adaptation; weak visibility; feasibility/complexity issues
Single-satellite	[7, 12]	1-sat association; limited coordination	No multi-connectivity; load imbalance; mobility sensitivity
Static multi-satellite	[8, 13, 14, 19, 20]	Multi-sat allowed; static/snapshot; heuristic visibility	Weak inter-slot coupling; high runtime; limited scalability
Long-term selection without RA	[9, 21–26]	Handover-centric; RSS/residual-time/prediction	No RA coupling; QoS/throughput gaps
Long-term selection with RA	[27–33]	Joint control; Lyapunov/DRL; architecture-specific	Training overhead; weak per-slot guarantees; partial visibility handling

2.2 Digital Twin in Satellites Network

Digital-twin (DT) concepts have recently been explored as an enabling layer for managing the high dynamics and operational complexity of LEO and satellite–terrestrial networks. Reference [34] proposes a hierarchical DT network tailored to satellite communication systems, where centralized and edge twins collaborate to support differentiated services and maintain synchronization under time-varying topology. A complementary vision is provided in [35], which articulates the motivations for DT-enabled satellite networks toward 6G, outlines a reference architecture, and highlights key challenges such as scalable model management, timely twin updates, and reliable closed-loop control. Beyond architectural perspectives, DTs have also been used to support concrete resource-management tasks: the authors in [36] study a DT-empowered satellite–terrestrial edge computing system and formulate multi-tier computation offloading with coupled delay/energy objectives, leveraging cooperative multi-agent deep reinforcement learning to adapt decisions to network dynamics. In a related direction, [37] focuses on contact-window resource scheduling with continuously arriving missions and rapidly changing satellite positions, introducing a dynamically updated DT/microcloud structure and an online scheduling strategy to improve resource utilization and revenue. DT assistance has also been investigated for mobility-aware storage and routing; specifically, [38] presents INTERLINK, which maps the satellite–terrestrial network into a virtual space to mitigate frequent handovers via storage-aware decisions, couples satellite selection with a multi-objective genetic algorithm, and further incorporates DT-assisted inter-satellite routing that accounts for time-varying link visibility. For real-time multi-beam operation in integrated SatCom, [39] advocates machine-learning-aided multibeam optimization to enable fast beam adaptation under large-scale coverage and dynamic conditions, which is compatible with DT-driven closed-loop network control. In addition to DT-centered designs, distributed intelligence mechanisms that can complement DT monitoring and decision loops have been discussed: [40] proposes federated learning for LEO-based satellite computing/communication networks to reduce satellite traffic while enabling distributed model training, and identifies key design issues on communication efficiency and resource management. Finally, DTs have

©2023-2027 SCION Consortium. All rights reserved.

also been extended to security, where [41] analyzes vulnerabilities in satellite Internet settings and outlines space-DT-enabled workflows for threat identification, risk assessment, and mitigation, pointing to a promising direction for building secure and reliable services.

Different from the above studies, DV-MOS2 does not assume fixed constellation or static satellite number. What's more, the proposed framework is designed based on the concept of Digital Twin to solve the problem of satellites selection. It is designed to handle dynamic visibility in M-LEO systems by jointly optimizing satellite selection, UA, and RA under constellation size constraints, combining Markov approximation with matching game theory to tackle the challenges of time-varying candidate satellite sets and coupled decision variables.

©2023-2027 SCION Consortium. All rights reserved.

3 System Model and Problem Formulation

3.1 Network Model

Consider the downlink of a M-LEO satellite network, in which satellites distributed across O orbital planes adaptively serve J UEs within a designated area, as illustrated in Fig. 1. Let $\mathcal{O} = \{1, \ldots, O\}$ and $\mathcal{U} = \{u_1, \ldots, u_J\}$ denote the sets of orbit indices and UE, respectively. Let $\mathcal{S} = \cup_{o=1}^{O} \mathcal{S}_o$ denote the set of satellites across O orbital planes, where $\mathcal{S}_o = \{s_{o,1}, \ldots, s_{o,|\mathcal{S}_o|}\}$ represents the set of satellites on the o-th orbital plane, and $|\mathcal{S}_o|$ denotes its cardinality. The downlink spectrum is assumed to be partitioned into K orthogonal and equal-bandwidth subcarriers, represented by the set $\mathcal{B} = \{B_1, \ldots, B_K\}$. For simplicity, we assume that all orbital planes share the same subcarrier set $\mathcal{B}$.

The framework of the system is shown in Fig. 2, where the physical world transmits the information of satellites' states and coordinates, power budget, and user communication rate to the digital replica in real time. After collecting and processing the real time data, the digital replica can make the decision based on the proposed algorithm and transmits the UA and RA strategy back the physical network. In our DT-assisted workflow, the Markov-approximation outer loop runs in the virtual entity VE and treats each feasible network configuration $f = \{\boldsymbol{x}, \boldsymbol{y}, \boldsymbol{z}, \boldsymbol{p}\}$ as a Markov state. At each time slot, the PE streams real-time satellite positions/states, power budgets, and observed user rates to the VE, which updates the candidate set and evaluates the utility $\theta(f)$ to compute transition probabilities between states. The selected state (satellite set and UA/RA decisions) is then sent back to the physical network for actuation, forming a closed-loop DT decision cycle.

3.2 Zenith Angle Rule

The zenith angle of the satellites relative to UE is an important metric for satellite selection, as it directly influence the communication quality in practical deployments [42]. To maintain line-of-sight (LoS) communication links, blockages caused by tall buildings should be avoided. A common method is to set up the threshold of the zenith angle when selecting satellites. Let φ denote the maximum zenith angle at which a UE can observe satellites. This threshold naturally defines a cone-shaped visibility region, and the satellites located within this cone for UE u_j constitute the candidate set, denoted as $\mathcal{S}_j(t)$. The cone-shaped visibility region and the corresponding candidate set $\mathcal{S}_j(t)$ are illustrated in Fig. 3. Based on the setup origin point, the coordinate values of u_j, $s_{o,i}$, and the earth center are denoted as $\boldsymbol{a}_j(t)$, $\boldsymbol{a}_{o,i}(t)$, and $\boldsymbol{a}_{\mathsf{e}}$, respectively. Accordingly, $\mathcal{S}_j(t)$ can be defined as

$$\mathcal{S}_j(t) = \{s_{o,i} \mid \langle \boldsymbol{a}_j(t) - \boldsymbol{a}_{\mathsf{e}}, \boldsymbol{a}_{o,i}(t) - \boldsymbol{a}_j(t) \rangle \leq \cos\varphi\}, \tag{1}$$

where $\langle \bullet, \bullet \rangle$ represents the calculation of the normalized inner product between two vectors.

All satellites located within the individual cone regions collectively form the union set, denoted as $\tilde{\mathcal{S}}(t) = \cup_j \mathcal{S}_j(t)$. The serving satellites are then selected from this candidate set. To indicate whether a specific satellite $s_{o,i}$ is actively providing service at time t, we introduce a binary decision variable $z_{o,i}(t) \in \{0, 1\}$, where its value is 1 i.i.f. the satellite is selected; otherwise, it evaluated to 0. The final set of optimized satellites is denoted as $\tilde{\mathcal{S}}^*(t) \subseteq \tilde{\mathcal{S}}^(t)$. Thus, the set of satellites providing service at time slot t is expressed as $\tilde{\mathcal{S}}^*(t) = \{s_{o,i} \mid z_{o,i}(t) = 1\}$.

In practical M-LEO operations, two edge cases may occur. First, if no satellite is visible for a UE under the zenith-angle rule, i.e., $\mathcal{S}_j(t) = \emptyset$, the UE cannot be scheduled in slot t and

©2023-2027 SCION Consortium. All rights reserved.

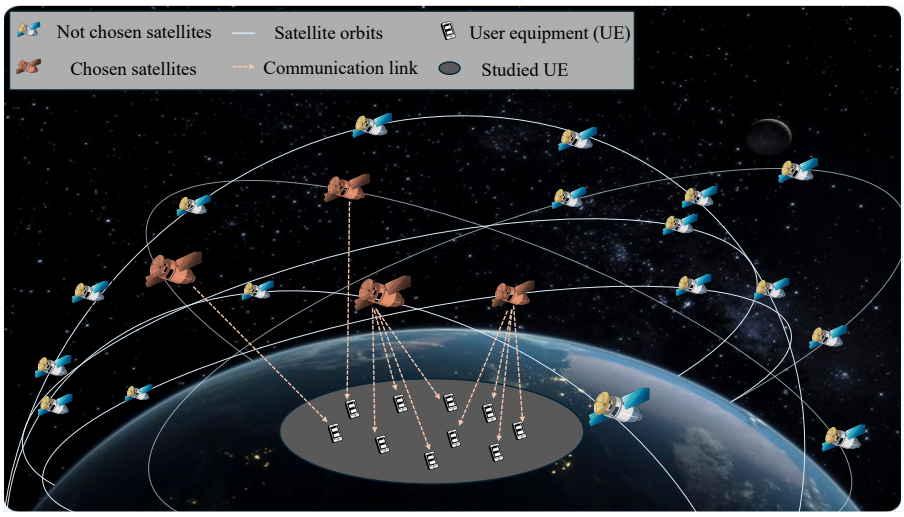


Figure 1: M-LEO satellite communication network.

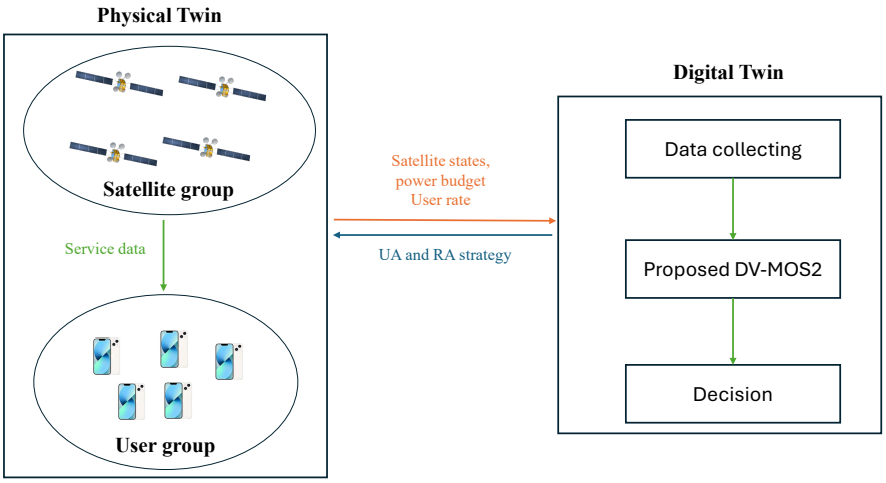


Figure 2: DT-assisted satellites communication network.

is marked as being in outage for this slot (equivalently, $r_j(t) = 0$). If the union candidate set is empty, i.e., $\tilde{\mathcal{S}}(t) = \emptyset$, the system experiences a temporary service outage in slot t and no UA/RA decision is executed.

Second, even when $\tilde{\mathcal{S}}(t) \neq \emptyset$, the minimum-rate QoS constraints may be infeasible due to limited bandwidth/power budgets or severe interference. In this case, the VE applies a graceful-degradation policy: it first attempts to find a feasible solution by reducing the scheduled UE set (e.g., prioritizing flows with stricter service requirements) while keeping per-satellite power budgets satisfied; if infeasibility persists, the system reports the violated QoS constraints and schedules the best-effort allocation for the remaining feasible users. The resulting outage/violation indicators are fed back to the DT for the next-slot decision update.

3.3 Transmission Model

It is important to note that only the satellites selected to provide service are eligible for bandwidth allocation (BA). The set of frequency bands assigned to $s_{o,i}$ is denoted by $\mathcal{B}_{o,i}$. The sets fulfill the conditions $\mathcal{B} = \cup_{s_{o,i} \in \tilde{\mathcal{S}}} \mathcal{B}_{o,i}(t)$, and $|\mathcal{B}_{o,i}(t)| = K/|\tilde{\mathcal{S}}^*(t)|$. We further assume that

©2023-2027 SCION Consortium. All rights reserved.

the frequency bands assigned to different service-providing satellites are mutually exclusive, i.e., there is no overlap between $\mathcal{B}_{o,i}(t)$ and $\mathcal{B}_{o,i'}(t)$ for $i \neq i'$. Formally, this condition is expressed as $\mathcal{B}_{o,i}(t) \cap \mathcal{B}_{o',i'}(t) = \emptyset, \forall (o,i) \neq (o',i')|_{z_{o,i}=z_{o',i'}=1}$. To characterize the connection relationships, we introduce two additional binary variables. The UA indicator is denoted as $x_{o,i,j}(t) \in \{0,1\}$, where $x_{o,i,j}(t) = 1$ if $s_{o,i}$ serves u_j at time slot t, and $x_{o,i,j}(t) = 0$ otherwise. Likewise, the BA is denoted as $y^k_{o,i,j}(t) \in 0,1$, with $y^k_{o,i,j}(t) = 1$ if frequency band B_k is allocated to serve u_j, and $y^k_{o,i,j}(t) = 0$ otherwise. Hence, the set of UE associated with $s_{o,i}$ is expressed as $\mathcal{U}_{o,i}(t) = \{u_j \mid x_{o,i,j}(t) = 1\}$, while the set of UE served by B_k is given by $\mathcal{U}_k(t) = \{u_j \mid y^k_{o,i,j}(t) = 1\}$.

The channel coefficient between u_j and $s_{o,i}$ at time t is

$$H_{o,i,j}(t) = \sqrt{PL_{o,i,j}(t) \cdot SF(t) \cdot G_t} h_{o,i,j}(t), \tag{2}$$

where G_t denotes the transmitting antenna gain, $SF(t)$ and $h_{o,i,j}(t)$ represent the shadowing fading and the small scale fading channel coefficient between $s_{o,i}$ and u_j, respectively. The path loss $PL_{o,i,j}(t)$ between $s_{o,i}$ and u_j is given by

$$PL_{o,i,j}(t) = C_1 \cdot \log_{10} d_{o,i,j}(t) + C_2 + C_3 \cdot \log_{10} f_c, \tag{3}$$

where $d_{o,i,j}(t)$ represents the Euclidean distance between $s_{o,i}$ and u_j, and f_c is the carrier frequency. The parameters C_1, C_2, and C_3 can be referred from tables provided in *QuaDRiGa* [43]. The small scale fading is calculated as $h_{o,i,j}(t) = e^{j2\pi f_c d_{o,i,j}(t)}$. The SINR experienced by u_j on the k-th subcarrier from its serving satellite $s_{o,i}$ at time t is

$$\Gamma^k_{o,i,j}(t) = x_{o,i,j}(t) \cdot y^k_{o,i,j}(t) \frac{p_j(t)|H^k_{o,i,j}(t)|^2}{I^k_{o,i,j}(t) + \sigma^2}, \tag{4}$$

where σ^2 is the noise level, $p_j(t)$ is u_j's transmit power, and

$$I^k_{o,i,j}(t) = \sum\nolimits_{j' \neq j} x_{o,i,j'}(t) y^k_{o,i,j'}(t) p_{j'}(t) |H^k_{o,i,j}(t)|^2, \tag{5}$$

is the multiple access interference experienced by u_j over B_k.

Thus, the rate of the network can be written as

$$R(t) = \sum\nolimits_{j=1}^{J} r_j(t), \tag{6}$$

where $r_j(t)$ is the data rate of u_j, given by

$$r_j(t) = \sum\nolimits_{o,i} x_{o,i,j}(t) r_{o,i,j}(t), \tag{7}$$

where $r_{o,i,j}(t)$ is the data rate of the communication link between $s_{o,i}$ and u_j, expressed as

$$r_{o,i,j}(t) = \sum\nolimits_{k=1}^{K} y^k_{o,i,j}(t) B \cdot \log_2 \left(1 + \Gamma^k_{o,i,j}(t)\right), \tag{8}$$

where B is the bandwidth value of one subcarrier. The definitions of variables are shown in Table 2.

©2023-2027 SCION Consortium. All rights reserved.

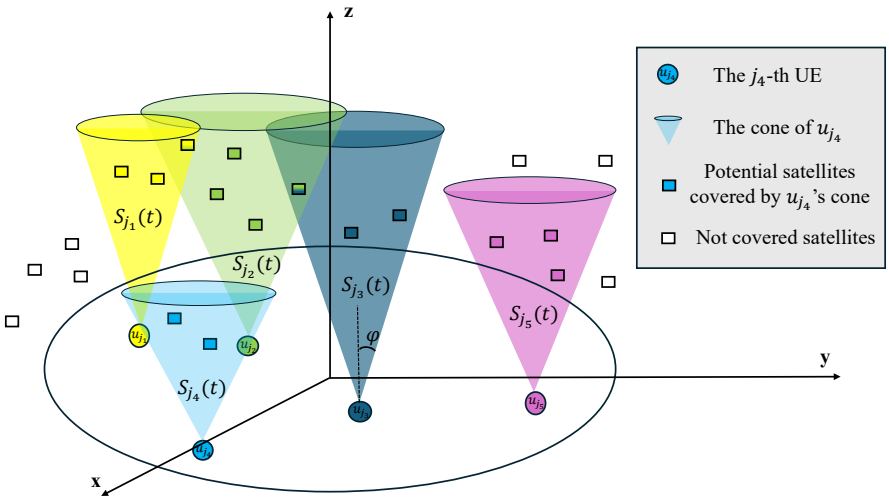


Figure 3: Illustration of the zenith angle rule.

3.4 Problem Formulation

Our setting explicitly accounts for dynamic visibility induced by each UE's cone-shaped field of view. As satellites on different orbital planes and relative phases enter/exit these cones, each per-UE candidate set $\mathcal{S}_j(t), \forall u_j \in \mathcal{U}$, along with their union $\tilde{\mathcal{S}}(t)$, evolves across time slots. Hence, both the number of serving satellites and their identities must be adapted online under constellation size limits and per-satellite power budgets. This time-varying feasible region tightly couples satellite selection, UA and PA, and substantially enlarges the combinatorial search space, motivating the problem formulation and algorithms that follow.

To summarize, the design of our problem setting encompasses both dynamic visibility and constellation size constraints, leading to the formulation of joint optimization problem that simultaneously addresses satellite selection, UA, and RA. Mathematically, this problem is

$$\textbf{OP-0}: \max_{\boldsymbol{x},\boldsymbol{y},\boldsymbol{z},\boldsymbol{p}} \quad \sum\nolimits_j r_j(t) \tag{9}$$

$$\text{s.t.} \quad \sum\nolimits_i x_{i,j}(t) \cdot z_i(t) \leq 1, \quad \forall j, \tag{10}$$

$$\sum\nolimits_{j=1}^{J} x_{i,j}(t) \cdot z_i(t) \cdot p_j(t) \leq P_{\max}, \quad \forall i, \tag{11}$$

$$\sum\nolimits_i z_i(t) \leq Z_{th}, \tag{12}$$

$$r_j(t) \geq r_{\min,j}(t), \quad \forall j, \tag{13}$$

$$p_j(t) > 0, \quad \forall j. \tag{14}$$

$$s_i(t) \in \tilde{\mathcal{S}}(t), \quad \forall (i)|_{z_i=1}, \tag{15}$$

$$x_{i,j}(t), y_j^k(t), z_i(t) \in \{0,1\}, \quad \forall i,j,k, \tag{16}$$

where (12) represents the constellation size constraint, which means that the number of the chosen satellites should not be larger than the threshold value Z_{th}. (15) guarantees that the serving satellites are selected from the union set defined by the cone-based visibility rule.

The optimization problem (9)-(16) is non-convex and mixed integer programming with respect to $\{\boldsymbol{x}, \boldsymbol{y}, \boldsymbol{z}, \boldsymbol{p}\}$, where $\boldsymbol{x} = [x_{o,i,j}]_{\forall o,i,j}$, $\boldsymbol{y} = [y^k_{o,i,j}]_{\forall o,i,j,k}$ and $\boldsymbol{z} = [z_{o,i}]_{\forall o,i}$, $\boldsymbol{p} = [p_j]_{\forall j}$. The problem involves integer constraints (10)-(12) and (15)-(16), as well as continuous constraints

©2023-2027 SCION Consortium. All rights reserved.

Table 2: Notation used in the network, visibility, and transmission models.

Symbol	Meaning
$\mathcal{O}$	Set of orbit indices.
$\mathcal{U}$	Set of UEs.
$\mathcal{S}$	Set of all satellites across O orbital planes.
$\mathcal{S}_o\}$	Set of satellites on the o-th orbital plane.
$\mathcal{B}$	Set of subcarriers.
B	Bandwidth of each subcarrier.
$\mathcal{S}_j(t)$	Candidate satellite set visible to UE u_j at time t (within zenith cone).
$\tilde{\mathcal{S}}(t)$	Union of all visible satellites over all UEs at time t.
$\tilde{\mathcal{S}}^*(t)$	Optimized set of selected satellites at time t.
$\mathcal{B}_{o,i}(t)$	Subcarrier set assigned to satellite $s_{o,i}$ at time t.
$\mathcal{U}_{o,i}(t)$	Set of UEs associated with satellite $s_{o,i}$ at time t.
$\mathcal{U}_k(t)$	Set of UEs served on subcarrier B_k at time t.
$H_{o,i,j}(t)$	Channel coefficient between $s_{o,i}$ and UE u_j at time t.
$PL_{o,i,j}(t)$	Path loss between $s_{o,i}$ and UE u_j at time t.
$SF(t)$	Shadowing fading factor at time t.
$h_{o,i,j}(t)$	Small-scale fading coefficient (phase term) between $s_{o,i}$ and UE u_j.
G_t	Transmit antenna gain.
$d_{o,i,j}(t)$	Euclidean distance between $s_{o,i}$ and UE u_j at time t.

(11) and (13)-(14). In the absence of efficient, general-purpose solvers for the exact problem, we adopt a tractable alternative. Specifically, we employ a problem-specific Markov approximation that exploits the combinatorial structure to deliver suboptimal solutions with manageable complexity; the methodology is detailed in the next section.

©2023-2027 SCION Consortium. All rights reserved.

4 The Proposed DV-MOS2 Framework

To effectively address problem (9)-(16), we propose the DV-MOS2 framework, which integrates three complementary components into a unified solution pipeline. First, a Markov approximation is employed to handle the combinatorial nature of satellite selection under constellation size constraints and dynamic visibility variations across time, reformulating the problem into a tractable form with guaranteed convergence to a stationary distribution. Next, based on the selected satellite set, a matching game is utilized to establish stable UA associations and BA. Finally, conditioned on the outcome, PA is optimized using KKT conditions. By combining these components in a sequential yet coherent manner, DV-MOS2 offers a scalable and near-optimal framework that achieves near-optimal performance for the joint problem of satellite selection and JUBPA, encompassing UA, BA, and PA. The overall workflow of DV-MOS2 is illustrated in Fig. 4, and the details of each component are elaborated in the following subsections.

4.1 Markov Approximation

Let $\boldsymbol{f} = \{\boldsymbol{x}, \boldsymbol{y}, \boldsymbol{z}, \boldsymbol{p}\} \in \mathcal{F}$ denote a feasible M-LEO satellites network configuration, with $\mathcal{F}$ as the feasible set. The objective function in (9) can then be expressed as $\theta(\boldsymbol{f}) = \sum_{t\in[0,T]} R(t)$ with $\boldsymbol{f} \in \mathcal{F}$. Accordingly, the original optimization problem can be equivalently written as

$$\max\nolimits_{\boldsymbol{f}\in\mathcal{F}} \quad \theta(\boldsymbol{f}). \tag{17}$$

Problem (17) is inherently discrete and combinatorial. To render it tractable, we approximate it by reformulating it into a continuous optimization problem through log-sum-exp relaxation and the use of a conjugate function [44]:

$$\max_{\boldsymbol{w}} \quad \sum_{\boldsymbol{f}_i\in\mathcal{F}} w_{\boldsymbol{f}_i}\theta(\boldsymbol{f}_i) - \frac{1}{\beta}\sum_{\boldsymbol{f}_i\in\mathcal{F}} w_{\boldsymbol{f}_i}\log(w_{\boldsymbol{f}_i}) \tag{18}$$

$$\text{s.t.} \quad \sum\nolimits_{\boldsymbol{f}_i\in\mathcal{F}} w_{\boldsymbol{f}_i} = 1, \tag{19}$$

where $w_{\boldsymbol{f}_i}$ denotes the weight of a feasible network configuration $\boldsymbol{f}_i$, β is a temperature parameter controlling the difference between the original problem and the transferred one. The KKT condition for (18) leads to an optimal variable as

$$w^*_{\boldsymbol{f}_i} = \frac{e^{\beta\theta(\boldsymbol{f}_i)}}{\sum_{m=1}^{|\mathcal{F}|} e^{\beta\theta(\boldsymbol{f}_m))}}. \tag{20}$$

All the feasible network configurations are needed to compute the optimal weight, which is not practical. To overcome this challenge, we view the feasible configurations as states and the corresponding weight as the stationary distribution of a Markov chain. The goal becomes the design of a Markov chain with the same state space and distribution as (20). There exists at least one Markov chain fulfilling our requirements [44].

The transition probability between two states $\boldsymbol{f}$ and $\boldsymbol{f}'$ can be calculated without considering all other states. Let $q(\boldsymbol{f} \to \boldsymbol{f}')$ and $q(\boldsymbol{f}' \to \boldsymbol{f})$ denote the transition probabilities. The Markov chain satisfies the balance condition, expressed as

$$w_{\boldsymbol{f}} q(\boldsymbol{f} \to \boldsymbol{f}') = w_{\boldsymbol{f}'} q(\boldsymbol{f}' \to \boldsymbol{f}), \tag{21}$$

$$e^{\beta\theta(\boldsymbol{f})} q(\boldsymbol{f} \to \boldsymbol{f}') = e^{\beta\theta(\boldsymbol{f}')} q(\boldsymbol{f}' \to \boldsymbol{f}), \tag{22}$$

©2023-2027 SCION Consortium. All rights reserved.

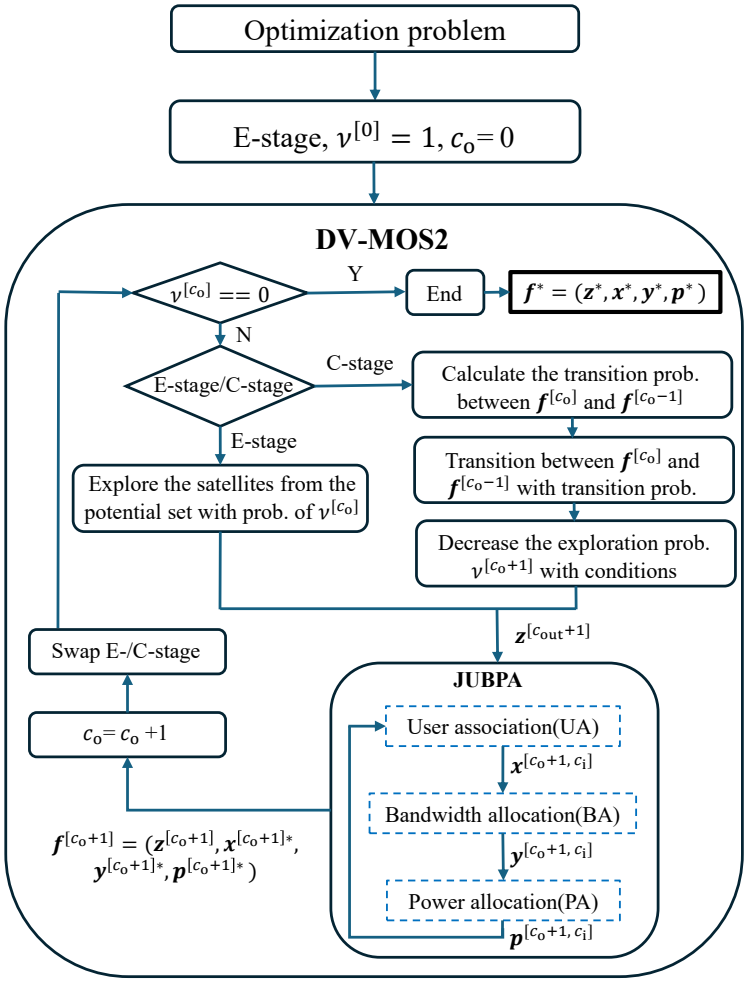


Figure 4: Overall workflow of the proposed DV-MOS2 framework.

where (21) is derived according to the Bayes rule on a joint probability of $\boldsymbol{f}$ and $\boldsymbol{f}'$, and (22) is obtained from (20) and (21). It is assumed that $q(\boldsymbol{f} \rightarrow \boldsymbol{f}') + q(\boldsymbol{f}' \rightarrow \boldsymbol{f}) = 1$, then the transition probabilities can expressed as

$$q(\boldsymbol{f} \rightarrow \boldsymbol{f}') = \frac{1}{1 + e^{\beta(\theta(\boldsymbol{f}) - \theta(\boldsymbol{f}'))}}, \tag{23}$$

$$q(\boldsymbol{f}' \rightarrow \boldsymbol{f}) = \frac{1}{1 + e^{\beta(\theta(\boldsymbol{f}') - \theta(\boldsymbol{f}))}}. \tag{24}$$

If the state stabilizes (i.e., remains unchanged across iterations), the exploration probability $\nu^{[c_o]}$ is gradually reduced. Finally, given the selected satellites, Algorithm 2 is invoked to determine the JUBPA.

Before executing Algorithm 2, it is necessary to find a feasibly initialized solution point. The idea here is to find the solution point at the boundary line generated by the minimum rate constraint (13), which means let the communication rate of each u_j equal to $r_{\text{min},j}$, i.e. $r_j(t) = r_{\text{min},j}(t)$. After substituting (8) into the equation and omitting the indexes o, i, t for simplicity, the equation can be rewritten as

$$B \cdot \log_2 \left[1 + \frac{p_j |H_j^k|^2}{\sum_{j', y_{j'}^k = 1} p_{j'} \cdot |H_j^k|^2 + \sigma^2} \right] = r_{\text{min},j}, \forall j, \tag{25}$$

©2023-2027 SCION Consortium. All rights reserved.

Algorithm 1 The DV-MOS2 Framework

Initialization: $c_{\mathsf{o}} = 0$, $\nu^{[0]} = 1$, $\beta_{\mathsf{step}} > 0$, $\nu_{\mathsf{step}} > 0$, $\boldsymbol{z}^{[0]}$ drawn at random.
while $\nu^{[c_{\mathsf{o}}]} \neq 0$ **do**
  if $\mod(c_{\mathsf{o}}, 2) = 0$ **then**
    % Exploration stage
    $\boldsymbol{z}^{[c_{\mathsf{o}}+1]} = \begin{cases} \boldsymbol{z} \quad \text{drawn randomly}, & \text{with prob. } \nu^{[c_{\mathsf{o}}]} \\ \boldsymbol{z}^{[c_{\mathsf{o}}]}, & \text{with prob. } 1-\nu^{[c_{\mathsf{o}}]} \end{cases}$
  else
    % Consolidation stage
    Calculate $\alpha = q(\boldsymbol{f}^{[c_{\mathsf{o}}]} \rightarrow \boldsymbol{f}^{[c_{\mathsf{o}}-1]})$
    $\boldsymbol{f}^{[c_{\mathsf{o}}+1]} = \begin{cases} \boldsymbol{f}^{[c_{\mathsf{o}}-1]}, & \text{with prob. } \alpha \\ \boldsymbol{f}^{[c_{\mathsf{o}}]}, & \text{with prob. } 1-\alpha \end{cases}$
    $\beta = \beta + \beta_{\mathsf{step}}$
    if $\boldsymbol{z}^{[c_{\mathsf{o}}+1]} = \boldsymbol{z}^{[c_{\mathsf{o}}]}$ **then**
      $\nu^{[c_{\mathsf{o}}+1]} = \max\left\{0, \nu^{[c_{\mathsf{o}}]} - \nu_{\mathsf{step}}\right\}$
  $\boldsymbol{f}^{[c_{\mathsf{o}}+1]*} = \left\{\boldsymbol{x}^{[c_{\mathsf{o}}+1]*}, \boldsymbol{y}^{[c_{\mathsf{o}}+1]*}, \boldsymbol{p}^{[c_{\mathsf{o}}+1]*}, \boldsymbol{z}^{[c_{\mathsf{o}}+1]}\right\}$ by running **JUBPA** reported in Algorithm 2
  $c_{\mathsf{o}} = c_{\mathsf{o}} + 1$
Return $\boldsymbol{z}^*$,$\boldsymbol{x}^*$,$\boldsymbol{y}^*$,$\boldsymbol{p}^*$

which is equivalent to

$$p_j \cdot \frac{1}{\delta_j} - \sum\nolimits_{j', y^k_{j'}=1} p_{j'} = \epsilon_{j,k}, \quad \forall j, \tag{26}$$

where $\delta_j = 2^{\frac{r_{j,\mathsf{min}}}{B}} - 1$, $\epsilon_{j,k} = \frac{\sigma^2}{|H^k_j|^2}$. It is obvious to see that based on (26), a system of first-degree linear equations for each subcarrier B_k can be generated as

$$G_k = G(\mathcal{U}_k) : \mathbf{A}_k \boldsymbol{p}_k = \boldsymbol{\epsilon}_k, \tag{27}$$

where $G(\cdot)$ is a function with the UE set receiving service from B_k and with the linear equations system as the output. The UE power vector $\boldsymbol{p}_k \in \mathbb{R}^{J_k \times 1}$ is defined as $[\boldsymbol{p}_k]_{j_k} = p_{j_k}$, $\boldsymbol{\epsilon}_k \in \mathbb{R}^{J_k \times 1}$

Algorithm 2 Algorithm of JUBPA

Ensure: $\boldsymbol{x}^{[c_{\mathsf{o}}+1]*}, \boldsymbol{y}^{[c_{\mathsf{o}}+1]*}, \boldsymbol{p}^{[c_{\mathsf{o}}+1]*}$
Require: $\boldsymbol{z}^{[c_{\mathsf{o}}+1]}$
for u_j in $\boldsymbol{L}^{\mathsf{init}}_{\mathsf{UE}}$ **do**
  for B_k in $\boldsymbol{L}^{\mathsf{init}}_j$ **do**
    if $G^+(G_k, u_j)$ is solvable **then**
      $\mathcal{U}_k \leftarrow \mathcal{U}_k \cup \{u_j\}$, Break
    else
      Continue
while $(\boldsymbol{x}, \boldsymbol{y})$ is not stable **do**
  UA+BA Phase: Run **Algorithm 3** and **Algorithm 4** to obtain $\boldsymbol{x}^{[c_{\mathsf{o}}+1,c_{\mathsf{i}}]}$ and $\boldsymbol{y}^{[c_{\mathsf{o}}+1,c_{\mathsf{i}}]}$
  PA Phase: Run **Algorithm 5** to obtain $\boldsymbol{p}^{[c_{\mathsf{o}}+1,c_{\mathsf{i}}]}$
  $c_{\mathsf{i}} = c_{\mathsf{i}} + 1$
Return $\boldsymbol{x}^{[c_{\mathsf{o}}+1]*}, \boldsymbol{y}^{[c_{\mathsf{o}}+1]*}, \boldsymbol{p}^{[c_{\mathsf{o}}+1]*}$

©2023-2027 SCION Consortium. All rights reserved.

is defined as $[\boldsymbol{\epsilon}_k]_{j_k} = \epsilon^k_{j_k}$. $J_k = \sum_{j_k} y^k_{j_k}$ is the number of UE accommodated by B_k. The matrix $\mathbf{A}_k \in \mathbb{R}^{J_k \times J_k}$ is defined as

$$[\mathbf{A}_k]_{ij} = \begin{cases} \frac{1}{\delta_j}, & i = j \\ -1, & i \neq j \end{cases}. \tag{28}$$

One more calculation should be defined to reflect the operation of trying to add u_j into the service list of B_k. The operation is defined as

$$G^+(G_k, u_j) : \mathbf{A}_{j\to k}\boldsymbol{p}_{j\to k} = \boldsymbol{\epsilon}_{j\to k}, \tag{29}$$

where $G^+(\cdot)$ is a function with the linear equations system relative to B_k and the newly added u_j as the input and with the updated linear equations system as the output. $\boldsymbol{p}_{j\to k} \in \mathbb{R}^{(J_k+1)\times 1}$ is defined as $\boldsymbol{p}_{j\to k} = [\boldsymbol{p}_k^T, p_j]^T$, $\boldsymbol{\epsilon}_{j\to k} \in \mathbb{R}^{(J_k+1)\times 1}$ is defined as $\boldsymbol{\epsilon}_{j\to k} = [\boldsymbol{\epsilon}_k^T, \epsilon_{j,k}]^T$. The updated matrix $\mathbf{A}_{j\to k} \in \mathbb{R}^{(J_k+1)\times(J_k+1)}$ is defined as

$$\left[\mathbf{A}_{j\to k}\right]_{i'j'} = \begin{cases} [\mathbf{A}_k]_{i'j'}, & i', j' \leq J_k \\ 1/\delta_j, & i' = j' = J_k + 1 \\ -1, & \text{others} \end{cases}. \tag{30}$$

The definition of solvable $G^+(G_k, u_j)$ is as the following

$$G^+(G_k, u_j) \text{ is solvable} \Longleftrightarrow \det\left(\mathbf{A}_{j\to k}\right) \neq 0, \left(\mathbf{A}_{j\to k}\right)^{-1} \boldsymbol{\epsilon}_{j\to k} > \mathbf{0}. \tag{31}$$

In the initialization of JUBPA, it should be emphasized that the UE with higher $r_{\mathsf{min},j}/\bar{g}_j(t)$ is prioritized to be allocated to its favorite subcarrier during initialization because the requirement of this kind of UE is difficult to achieve. When hitting into the loop of accommodating UE, whether the minimum rate requirement of the accommodated UE is fulfilled is checked, which means only if the new UE does not influence the other accommodated UE's requirement, it can be accommodated into the current subcarrier.

4.2 Matching Game Theory

All the matching games are designed based on the explored $\boldsymbol{z}^{[c_0+1]}$ and the corresponding set of satellites is defined as $\mathcal{S}_{\boldsymbol{z}^{[c_0+1]}}(t)$. For simplicity, it will be denoted as $\mathcal{S}_{\boldsymbol{z}}(t)$ in the coming text. The matching $\mu_{\mathsf{UA}}(\cdot)$ for UA is defined as a mapping function from the set $\mathcal{U}$ to the set $\mathcal{S}_{\boldsymbol{z}}(t)$ such that $s_{o,i} = \mu_{\mathsf{UA}}(u_j)$ i.i.f. $u_j \in \mu^{-1}_{\mathsf{UA}}(s_{o,i})$, where combined with the definition of $x_{o,i,j}$, $\mu^{-1}_{\mathsf{UA}}(s_{o,i})$ is defined as

$$\mu^{-1}_{\mathsf{UA}}(s_{o,i}; t) = \mathcal{U}_{o,i} = \left\{u_j \mid x_{o,i,j}(t) = 1\right\}. \tag{32}$$

Likewise, the matching $\mu_{\mathsf{BA}}(\cdot)$ for BA is defined as a function from the set $\mathcal{U}_{o,i}$ to the set $\mathcal{B}_{o,i}$ such that $B_k = \mu_{\mathsf{BA}}(u_j)$ i.i.f. $u_j \in \mu^{-1}_{\mathsf{BA}}(B_k)$, where combined with the definition of $y^k_{o,i,j}$, $\mu^{-1}_{\mathsf{BA}}(B_k)$ is defined as

$$\mu^{-1}_{\mathsf{BA}}(B_k; t) = \mathcal{U}_k = \{u_j \mid y^k_{o,i,j}(t) = 1\}. \tag{33}$$

The UA and BA parts are designed to solve the following sub-problem

$$\textbf{OP-UABA} : \max_{\boldsymbol{x},\boldsymbol{y}} \quad R(t) \tag{34}$$

$$\text{s.t. (10), (11), (13), (16).} \tag{35}$$

©2023-2027 SCION Consortium. All rights reserved.

Algorithm 3 Algorithm of UA

Ensure: $\boldsymbol{x}^{[c_o+1,c_i]}$,$\boldsymbol{y}^{[c_o+1,c_i]}$
Require: $\boldsymbol{x}^{[c_o+1,c_i-1]}$, $\boldsymbol{y}^{[c_o+1,c_i-1]}$, $\boldsymbol{p}^{[c_o+1,c_i-1]}$
for each u_j **do**
  Update $\boldsymbol{L}_j^{\mathsf{UA},[c_{\mathsf{in}}]}$ based on $PF_j^{\mathsf{UA}}(o,i;\boldsymbol{\mu}^{[c_{\mathsf{in}}-1]})$
while $\mathcal{U}_{\mathsf{req}}^{\mathsf{UA}} \neq \emptyset$ **do**
  for $u_j \in \mathcal{U}_{\mathsf{req}}^{\mathsf{UA}}$ **do**
    if $U_j \leq U_{q_j}$ and $\mu_{\mathsf{UA}}(u_j) \neq s_{o^*,i^*}$ **then**
      $o^*, i^* = \arg\max_{s_{o,i} \in \boldsymbol{L}_j^{\mathsf{UA}}} PF_j^{\mathsf{UA}}(o,i)$,$b_{j\to o^*,i^*} = 1$
  for each $s_{o,i} \in \mathcal{S}_{\boldsymbol{z}}$ **do**
    $U_{o,i}^{\mathsf{req}} = \{u_j \mid b_{j\to(o,i)} = 1\}$,$p_{o,i}^{\mathsf{req}} = \sum_{u_j \in \mathcal{U}_{o,i}^{\mathsf{req}}} p_j$
    if $p_{o,i} + p_{o,i}^{\mathsf{req}} \leq p_{\mathsf{max}}$ **then**
      $\mathcal{U}_{o,i} \leftarrow \mathcal{U}_{o,i}^{\mathsf{req}} \cup \mathcal{U}_{o,i}$, $p_{o,i} += p_{o,i}^{\mathsf{req}}$, $\mathcal{U}_{o,i}^{\mathsf{req}} \leftarrow \emptyset$,$\mathcal{U}_{\mathsf{req}}^{\mathsf{UA}} \leftarrow \mathcal{U}_{\mathsf{req}}^{\mathsf{UA}} \setminus \{u_j \mid u_j \in \mathcal{U}_{\mathsf{req}}^{\mathsf{UA}}\}$
    else
      while $p_{o,i} < p_{\mathsf{max}}$ **do**
        $j' = \arg\max_{u_j \in \boldsymbol{L}_{o,i}^{\mathsf{UA}}} \sum_{j \in \mathcal{U}_{o,i}} PF_{o,i}^{\mathsf{UA}}(j)$, $\mathcal{U}_{o,i} \leftarrow \mathcal{U}_{o,i} \cup \{u_{j'}\}$, $p_{o,i} \leftarrow p_{o,i} + p_{j'}$, $\mathcal{U}_{\mathsf{req}}^{\mathsf{UA}} \setminus \{u_{j'}\}$,$\mathcal{U}_{o,i}^{\mathsf{req}} \setminus \{u_{j'}\}$,$\boldsymbol{L}_{o,i}^{\mathsf{UA}} \setminus \{u_{j'}\}$
    for $u_j \in \mathcal{U}_{o,i}^{\mathsf{rej}}$ **do**
      $\boldsymbol{L}_j^{\mathsf{UA},[c_{\mathsf{in}}]} \leftarrow \boldsymbol{L}_j^{\mathsf{UA},[c_{\mathsf{in}}]} \setminus \{s_{o,i}\}$
for $s_{o,i} \in \mathcal{S}^{\mathsf{UA},[c_i]}$ **do**
  The list $\boldsymbol{L}_{o,i}^{\mathsf{UA},[c_i]} = \mathrm{argsort}_{u_j \in \mathcal{U}_{o,i}^{\mathsf{UA},[c_i]}} p_j(t)$
  for $u_j \in \boldsymbol{L}_{o,i}^{\mathsf{UA},[c_i]}$ **do**
    The sorted list $\boldsymbol{L}_j^{o,i} = \mathrm{argsort}_{B_k \in \mathcal{B}_{o,i}} g_j^k(t)$
    for $B_k \in \boldsymbol{L}_j^{o,i}$ **do**
      if r_{min} constraint in B_{k^*} is fulfilled **then**
        $y_{o,i,j}^k(t) = 1$
      else
        $x_{o,i,j}(t) = 0, x_{o,i,j}^{[c_i-1]} = 1, U_j -= 1$

The final matching result of two procedures is denoted as $\boldsymbol{\mu} = \{\mu_{\mathsf{UA}}, \mu_{\mathsf{BA}}\}$. In the stage of UA, we try to obtain the mapping relationship between the picked satellites and UE. Two profile lists for two sides of agents will be constructed. Profiles lists on UE side which sort the satellites are used to deal with the objective function in the problem. Profile lists on satellites side which sort different UE are used to cope with the minimum rate constraints in the problem. After constructing these two profile lists, we can guarantee that the found solution can fall in the feasible set and be close to the optimal objective value. These two profile lists will be constructed based on the following two preference functions, which can be viewed as the criteria for UE/satellites to choose satellites/UE to connect.

4.2.1 User Association

In the game theory, it is UE side that proposes the association changing requirement in the first place, so we make the profile list on UE side deal with the objective function in the optimization problem. In order to make the function value increase after each iteration as much as possible, the preference function should be designed based on the increment of

©2023-2027 SCION Consortium. All rights reserved.

Algorithm 4 Algorithm of BA

for each $s_{o,i} \in \mathcal{S}_{\boldsymbol{z}}$ **do**
  while $\max PF^{\mathsf{BA}}(j,k) > 0$ **do**
    $\mathcal{U}_{\mathsf{req}}^{\mathsf{BA}} \leftarrow \emptyset$,$\mathcal{B}_{\mathsf{block}} \leftarrow \emptyset$
    for each $B_k \in \mathcal{B}_{o,i}$ **do**
      $\mathcal{U}_{\mathsf{req}}^{\mathsf{BA}} \leftarrow \mathcal{U}_{\mathsf{req}}^{\mathsf{BA}} \cup \left\{\arg\min_{u_j \in \mathcal{U}_k} r_j(t)\right\}$
    while $\max \boldsymbol{L}^{\mathsf{BA}} \geq 0$ **do**
      $(j^*, k^*) = \arg\max_{j,k \in \boldsymbol{L}^{\mathsf{BA}}} PF^{\mathsf{BA}}(j,k)$
      if $\left\{\mu^{\mathsf{BA}}(j^*), B_{k^*}\right\} \notin \mathcal{B}_{\mathsf{block}}$ **then**
        if the r_{min} constraint in B_{k^*} is fulfilled **then**
          $\mathcal{U}_{k^*} \leftarrow \mathcal{U}_{k^*} \cup u_{j^*}$,$\mathcal{U}_{\mu^{\mathsf{BA}}(j^*)} \leftarrow \mathcal{U}_{\mu^{\mathsf{BA}}(j^*)} \setminus j^*$, $\mathcal{B}_{\mathsf{block}} \leftarrow \mathcal{B}_{\mathsf{block}} \cup \left\{\mu^{\mathsf{BA}}(j^*), B_{k^*}\right\}$
        $\boldsymbol{L}^{\mathsf{BA}} \leftarrow \boldsymbol{L}^{\mathsf{BA}} \setminus \left\{(j^*, k^*)\right\}$

each UE's communication rate. To describe the rate change after changing the association relationship, the rate function of u_j after putting u_j into B_k is defined as

$$r_{j\to k}(t) = B \cdot \log_2\left(1 + \frac{p_j(t) \cdot |H_j^k(t)|^2}{\sum_{j' \in \mathcal{U}_k} p_{j'}(t) \cdot |H_j^k(t)|^2 + \sigma^2}\right), \tag{36}$$

where it does not mean u_j will be actually served by B_k. In order to define the expression of the preference function, the set of subcarriers which can make the communication rate of u_j higher after accommodating u_j is defined as

$$\mathcal{B}_{j\to o,i}^{+} = \left\{B_k \mid r_{j\to k}(t) \geq r_j(t), B_k \in \mathcal{B}_{o,i}\right\}. \tag{37}$$

The definition of profile function of u_j is defined as

$$PF_j^{\mathsf{UA}}(o,i;\boldsymbol{\mu},t) = \frac{1}{|\mathcal{B}_{j\to o,i}^{+}|} \sum_{k \in \mathcal{B}_{j\to o,i}^{+}} \left(r_{j\to k}(t) - r_j(t)\right), \tag{38}$$

which means that if all the effective subcarriers on the satellite $s_{o,i}$ could provide higher SINR to u_j, then the satellite will be preferred by u_j. The comparison operator for u_j at UA stage is defined based on the preference function as

$$(s_{o,i}, \mu_{\mathsf{UA}}) \succ_{j;t}^{\mathsf{UA}} (s_{o',i'}, \mu'_{\mathsf{UA}}) \Leftrightarrow PF_j^{\mathsf{UA}}(o,i;\boldsymbol{\mu},t) \geq PF_j^{\mathsf{UA}}(o',i';\boldsymbol{\mu}',t). \tag{39}$$

Profile lists on the UE side are denoted by $\boldsymbol{L}_j^{\mathsf{UA}}(t)$. Each $\boldsymbol{L}_j^{\mathsf{UA}}(t)$ represents an ordered list of satellites, arranged in descending order according to the preference function $PF_j^{\mathsf{UA}}(o,i)$.

$$\boldsymbol{L}_j^{\mathsf{UA}}(t) = \underset{s_{o,i} \in \mathcal{S}_{\boldsymbol{z}}}{\operatorname{argsort}} \quad PF_j^{\mathsf{UA}}(o,i). \tag{40}$$

The maximum achievable rate of u_j can be derived from $\gamma_j(t) = \max_{s_{o,i} \in \boldsymbol{L}_j^{\mathsf{UA}}(t)} PF_j^{\mathsf{UA}}(o,i)$.

It is important to make the algorithm converge. The condition of the interference calculation in each subcarrier will be changed after accommodating new u_j, so we need to control the

©2023-2027 SCION Consortium. All rights reserved.

amount of UE which can attend the change of UA to avoid the large change of the accommodation condition. First we need to define the sorted list $\boldsymbol{L}^{\gamma}$ with UE as the elements which is sorted based on $\gamma_j(t)$ and it is defined as

$$\boldsymbol{L}^{\gamma}(t) = \underset{u_j \in \mathcal{U}}{\text{argsort}} \quad \gamma_j(t). \tag{41}$$

Here we define this quota value as U_q. The U_q UEs which have the largest value of $\gamma_j(t)$ are allowed to attend the UA change. In the algorithm, the set of u_j which is allowed to propose the requirement of changing the serving satellite is denoted as $\mathcal{U}_{\text{req}}^{\text{UA}}$ and it is defined as

$$\mathcal{U}_{\text{req}}^{\text{UA}} = \{u_{(j)} \in \boldsymbol{L}^{\gamma}(t) \mid 1 \leq j \leq U_q\}. \tag{42}$$

At the same time, how many times single UE can change the UA should also be controlled, the quota here is denoted as U_{q_j}. To build the preference function and the profile list for the satellites at UA stage, the constraint (13) is rewritten as

$$p_j(t)|H_j^k(t)|^2 \geq \epsilon_{j,k} + \sum_{\substack{j' \neq j \\ \mu(u_{j'};t)=B_k}} \delta_j \cdot p_{j'}(t)|H_j^k(t)|^2 \tag{43}$$

and

$$p_j(t)/\delta_j - \epsilon_{j,k} \geq \sum\nolimits_{j' \neq j, \mu(u_{j'};t)=B_k} p_{j'}(t), \tag{44}$$

where for all UE, the term $p_j(t)/\delta_j - \epsilon_{j,k}$ is the advantage of u_j which means that if this term is larger, it will be easier to fulfill the constraint. The transmitted power of u_j, $p_j(t)$ is the negative influence which is brought by u_j to other UE. Based on the above discussion, the preference function of $s_{o,i}$ is defined as

$$PF_{o,i}^{\text{UA}}(j;t) = \varphi_{\text{UA}} \sum_{k \in \mathcal{B}_{o,i}} \left(\frac{p_j(t)}{\delta_j} - \epsilon_{j,k} \right) - \sum_{k \in \mathcal{B}_{o,i}} c_k \cdot p_j(t), \tag{45}$$

where φ_{UA} is the coefficient capturing the benefit of u_j, c_k is the cost per unit of the interference caused by u_j [45]. The PF here quantifies how attractive a candidate is by balancing a *benefit term* (achievable rate / channel quality) against a *cost term* (interference caused to others or resource consumption). Hence, a larger PF indicates that selecting this association/resource yields higher net gain under the current network state.

Similarly, the corresponding comparison function for satellites is obtained as

$$(j, \mu_{\text{UA}}) \succ_{o,i;t}^{\text{UA}} (j', \mu'_{\text{UA}}) \Leftrightarrow PF_{o,i}^{\text{UA}}(j;t) \geq PF_{o,i}^{\text{UA}}(j';t). \tag{46}$$

Profiles lists of $s_{o,i}$ which sort the UE are used to cope with the constraints in the problem, which is denoted as $\boldsymbol{L}_{o,i}^{\text{UA}}(t)$. Likewise, it can be defined as

$$\boldsymbol{L}_{o,i}^{\text{UA}}(t) = \underset{u_j \in \mathcal{U}_{o,i}}{\text{argsort}} \quad PF_{o,i}^{\text{UA}}(j). \tag{47}$$

After executing the c_i-th round of algorithm, it is natural to generate the set of UE which changes the serving satellites as

$$\mathcal{U}_{o,i}^{\text{UA},[c_i]} = \left\{ u_j \mid x_{o,i,j}^{[c_o+1,c_i]}(t) = 1, x_{o,i,j}^{[c_o+1,c_i-1]}(t) = 0 \right\}. \tag{48}$$

The set of satellites which serve new satellites is defined as

$$\mathcal{S}^{\text{UA},[c_i]} = \{s_{o,i} \mid \mathcal{U}_{o,i}^{\text{UA},[c_i]} \neq \emptyset\}. \tag{49}$$

©2023-2027 SCION Consortium. All rights reserved.

4.2.2 Bandwidth Allocation

In the BA part, because the change of channel bandwidth accommodating will influence two frequency bands, we need to update the profile based on the network status after each single variation. One UE moving to a new subcarrier will cause the sum rate to be increased in the original subcarrier but decreased in the new subcarrier. Before conducting the BA, it is necessary to accommodate the UE which changed the UA relationship in the UA stage.

In order to describe the profile function, a function to describe a sum rate function of each subcarrier needs to be introduced. It is obvious that the sum rate within each subcarrier is decided by the accommodated UE in it. So the function of calculating the sum rate of B_k based on any UE set $\mathcal{U}_x$ is defined as

$$R_k\left(\mathcal{U}_x\right) = \sum\nolimits_{j\in\mathcal{U}_x} B \times \log_2\left[1 + \frac{p_j(t)|H_j^k(t)|^2}{\sum_{j'\neq j, j'\in\mathcal{U}_x} p_{j'}(t)|H_j^k(t)|^2 + \sigma^2}\right].$$

We denote the set of UE without u_j in B_k as $\mu_{\mathsf{BA}}^{-1}(k)\backslash j$ and the set with u_j involved as $\mu_{\mathsf{BA}}^{-1}(k)\cup u_j$. Based on the above mentioned rules, the accommodation of one UE changes from one subcarrier to another can result in two facts, the rate of other UE in the original subcarrier increases and the sum rate of other UE in the new subcarrier decreases. The first profile function is defined as

$$PF1^{\mathsf{BA}}(j;\boldsymbol{\mu}) = R_{\mu_{\mathsf{BA}}(j)}\left(\mu_{\mathsf{BA}}^{-1}(\mu_{\mathsf{BA}}(j)) \setminus j\right) - R_{\mu_{\mathsf{BA}}(j)}. \tag{50}$$

The second profile function is defined as

$$PF2^{\mathsf{BA}}(j,k;\boldsymbol{\mu}) = R_k\left(\mu_{\mathsf{BA}}^{-1}(k) \cup j\right) - R_k. \tag{51}$$

The final profile function can be defined as

$$PF^{\mathsf{BA}}(j,k;\boldsymbol{\mu}) = PF1^{\mathsf{BA}}(j;\boldsymbol{\mu}) + PF2^{\mathsf{BA}}(j,k;\boldsymbol{\mu}). \tag{52}$$

The sorted profile can be constructed based on $PF(j,k;\boldsymbol{\mu})$ which is defined as $\boldsymbol{L}^{\mathsf{BA}}$. It should be emphasized that the second profile list is constructed for two indexes j and k. It is calculated as

$$\boldsymbol{L}_{o,i}^{\mathsf{BA}}(t) = \underset{u_j\in\mathcal{U}_{o,i}, B_k\in\mathcal{B}_{o,i}}{\operatorname{argsort}} \quad PF^{\mathsf{BA}}(j,k). \tag{53}$$

Theorem 1. *The matching $\boldsymbol{\mu} = \{\mu_{UA}, \mu_{BA}\}$ is stable and can capture a local optimal solution given the transmitted power.*

Proof. See Appendix 7.1.

□

4.3 Lagrangian Dual-Based Optimization for PA

After UA and BA stages, the original optimization problem can be formulated as

$$\textbf{OP-PA0}_{s_{o,i}}: \max_{\boldsymbol{p}} \quad \sum\nolimits_{j\in\mathcal{U}_{o,i}} \log_2\left(1+\Gamma_j^k\right) \tag{54}$$

$$\text{s.t.} \ \sum\nolimits_{j\in\mathcal{U}_{o,i}} p_j \leq P_{\mathsf{max}}, \tag{55}$$

$$r_j \geq r_{\mathsf{min},j}, \quad \forall j \in \mathcal{U}_{o,i}, \tag{56}$$

$$p_j \geq 0, \quad \forall j \in \mathcal{U}_{o,i}. \tag{57}$$

©2023-2027 SCION Consortium. All rights reserved.

The problem is decomposed into several sub-problems with each sub-problem corresponding to one satellite. Then we can transfer this problem into the following one through geometrical programming. Let $\log_2\left(1+\Gamma_j^k(t)\right) \simeq \log_2\left(\Gamma_j^k(t)\right)$ and let $\acute{p}_j = \log_2 p_j$. Another approximation is introduced here, let $\acute{I}_j^k = \log_2 I_j^k$. Then **PA-0**$_{s_{o,i}}$ is transformed as

$$\textbf{OP-PA1}_{s_{o,i}}: \min_{\acute{\boldsymbol{p}},\acute{\boldsymbol{I}}} \quad \sum\nolimits_{j\in\mathcal{U}_{o,i}} \log_2\left[\frac{2^{-\acute{p}_j}}{|H_j^k|^2}(2^{\acute{I}_j^k}+\sigma^2)\right] \tag{58}$$

$$\text{s.t. } \sum\nolimits_{j\in\mathcal{U}_{o,i}} 2^{\acute{p}_j} \le P_{\max}, \tag{59}$$

$$\log_2\left[\frac{2^{-\acute{p}_j}(2^{\acute{I}_j^k}+\sigma^2)}{|H_j^k(t)|^2}\right] + \chi_j \le 0, \quad \forall j \in \mathcal{U}_{o,i}, \tag{60}$$

$$-\acute{I}_j^k + \log_2 I_j^k = 0, \quad \forall j \in \mathcal{U}_{o,i}. \tag{61}$$

where $\chi_j = \frac{r_{\min,j}}{B}$, $\forall j \in \mathcal{U}_{o,i}$. It should be noticed that I_j^k should be viewed as a function of $\acute{\boldsymbol{p}}$, which means that I_j^k will be updated based on the values of $\acute{\boldsymbol{p}}$. With the constraint (61), it can be guaranteed we can solve out the same values of optimal $\acute{\boldsymbol{p}}$ through the values of $\acute{\boldsymbol{I}}$.

The original problem can be transferred into

$$\textbf{OP-PA2}_{s_{o,i}}: \min_{\acute{\boldsymbol{p}},\acute{\boldsymbol{I}}} \max_{\lambda_{o,i},\boldsymbol{n},\boldsymbol{m}} \quad L_{o,i} \tag{62}$$

$$\text{s.t. } \lambda_{o,i} \ge 0, \boldsymbol{n} \ge \boldsymbol{0}, \boldsymbol{m} \ge \boldsymbol{0}, \tag{63}$$

where the Lagrange term $L_{o,i}$ can be calculated as

$$\begin{aligned} L_{o,i} = &\sum_{j\in\mathcal{U}_{o,i}} \log_2\left[\frac{2^{-\acute{p}_j}}{|H_j^k|^2}(2^{\acute{I}_j^k}+\sigma^2)\right] \\ &+ \lambda_{o,i}\left(\sum\nolimits_{j\in\mathcal{U}_{o,i}} 2^{\acute{p}_j} - P_{\max}\right) \\ &+ \sum_{j\in\mathcal{U}_{o,i}} n_j\left(\log_2\left[\frac{2^{-\acute{p}_j}}{|H_j^k|^2}(2^{\acute{I}_j^k}+\sigma^2)\right] + \chi_j\right) \\ &+ \sum\nolimits_{j\in\mathcal{U}_{o,i}} m_j(-\acute{I}_j^k + \log_2 I_j^k). \end{aligned} \tag{64}$$

The duality function can be defined as $D_{o,i}(\lambda_{o,i},\boldsymbol{n},\boldsymbol{m}) = \min_{\acute{\boldsymbol{p}},\acute{\boldsymbol{I}}} L_{o,i}$. Then the duality problem can be defined as

$$\textbf{PA-3}_{s_{o,i}}: \max_{\lambda_{o,i},\boldsymbol{n},\boldsymbol{m}} \quad D_{o,i}(\lambda_{o,i},\boldsymbol{n},\boldsymbol{m}) \tag{65}$$

$$\text{s.t. } \lambda_{o,i} \ge 0, \boldsymbol{n} \ge \boldsymbol{0}, \boldsymbol{m} \ge \boldsymbol{0}, \tag{66}$$

which is equivalent to the original problem because the strong duality holds here.

According to the KKT condition, the derivative of transmitted power and interference can be calculated as

$$\partial L_{o,i}/\partial \acute{p}_j = -(1+n_j) + \lambda_{o,i} 2^{\acute{p}_j}\cdot \ln 2, \tag{67}$$

$$\partial L_{o,i}/\partial \acute{I}_j^k = (1+n_j)2^{\acute{I}_j^k}/(2^{\acute{I}_j^k}+\sigma^2) - m_j. \tag{68}$$

©2023-2027 SCION Consortium. All rights reserved.

Algorithm 5 Algorithm of PA

Ensure: $\boldsymbol{p}^{[c_0+1,c_1]}$
Require: $\boldsymbol{x}^{[c_0+1,c_1]}, \boldsymbol{y}^{[c_0+1,c_1]}, \boldsymbol{p}^{[c_0+1,c_1-1]}$
1: **Initialization:** $\boldsymbol{\lambda}^{(0)}, \boldsymbol{n}^{(0)}, \boldsymbol{m}^{(0)}, \boldsymbol{p}^{(0)}, \boldsymbol{I}^{(0)}$
2: **for** each $s_{o,i} \in \mathcal{S}_{\boldsymbol{z}}$ **do**
3: $r = 0$
4: **while** $\acute{\boldsymbol{p}}$ does not converge **do**
5: **if** r == 0 **then**
6: Update $\lambda_{o,i}^{(1)}$, $n_j^{(1)}$ and $m_j^{(1)}$ according to (73), (74) and (75) based on the values of $\boldsymbol{p}^{(0)}, \boldsymbol{I}^{(0)}$
7: **else**
8: Update $\acute{p}_j^{(r)*}$ and $\acute{I}_j^{k,(r)*}$ based on (69) and (70)
9: Calculate the value of $I_j^{k,(r)}$ based on the value of $\acute{\boldsymbol{p}}^{(r)*}$ according to (5)
10: Update $\lambda_{o,i}^{(r+1)}$, $n_j^{(r+1)}$ and $m_j^{(r+1)}$ according to (73), (74) and (75) based on the values of $\acute{\boldsymbol{p}}^{(r)*}$, $I_j^{k,(r)}$ and $\acute{I}_j^{k,(r)*}$
11: $r = r + 1$

Then the optimal value of power and interference are

$$p_j^* = 2^{\acute{p}_j^*} = (1 + n_j)/(\lambda_{o,i} \ln 2), \tag{69}$$

$$I_j^{k*} = 2^{\acute{I}_j^{k*}} = \max\{m_j \sigma^2/(1 + n_j - m_j), 0\}. \tag{70}$$

It should be emphasized that the values of $\acute{\boldsymbol{p}}$ and $\acute{\boldsymbol{I}}$ are calculated based on the Lagrange multipliers, but during the following stage of updating the multipliers, the values of $\acute{\boldsymbol{p}}$ and $\acute{\boldsymbol{I}}$ will be still kept as the constants without being changed with the values of multipliers. $D_{o,i}(\lambda_{o,i}, \boldsymbol{n}, \boldsymbol{m})$ can be defined as

$$D_{o,i}(\lambda_{o,i}, \boldsymbol{n}, \boldsymbol{m}) = L_{o,i}(\lambda_{o,i}, \boldsymbol{n}, \boldsymbol{m}; \acute{\boldsymbol{p}}^*, \acute{\boldsymbol{I}}^*). \tag{71}$$

As a result, $f_{o,i}(\lambda_{o,i}, \boldsymbol{n}, \boldsymbol{m})$ can be defined as

$$f_{o,i}(\lambda_{o,i}, \boldsymbol{n}, \boldsymbol{m}) = -L_{o,i}(\lambda_{o,i}, \boldsymbol{n}, \boldsymbol{m}; \acute{\boldsymbol{p}}^*, \acute{\boldsymbol{I}}^*). \tag{72}$$

Lagrange multipliers $\lambda_{o,i}$, n_j and m_j can be updated recursively with step sizes $q_\lambda^{(r)}$, $q_n^{(r)}$ and $q_m^{(r)}$ according to the subgradient method as

$$\lambda_{o,i}^{(r)} = \lambda_{o,i}^{(r-1)} + q_\lambda^{(r)} \cdot g_{\lambda_{o,i}}^{(r-1)}, \tag{73}$$

$$n_j^{(r)} = n_j^{(r-1)} + q_{n_j}^{(r)} \cdot g_{n_j}^{(r-1)}, \tag{74}$$

$$m_j^{(r)} = m_j^{(r-1)} + q_{m_j}^{(r)} \cdot g_{m_j}^{(r-1)}, \tag{75}$$

where

$$g_{\lambda_{o,i}}^{(r-1)} = \sum\nolimits_{j \in \mathcal{U}_{o,i}} 2^{\acute{p}_j^{(r-1)*}} - P_{\max}, \tag{76}$$

$$g_{n_j}^{(r-1)} = \log_2 \left[\frac{2^{-\acute{p}_j^{(r-1)*}}}{|H_j^k|^2} (2^{\acute{I}_j^{k,(r-1)*}} + \sigma^2) \right] + \chi_j, \tag{77}$$

$$g_{m_j}^{(r-1)} = \log_2 \left[I_j^{k,(r-1)}(\acute{\boldsymbol{p}}^{(r-1)*}) \right] - \acute{I}_j^{k,(r-1)*}, \tag{78}$$

©2023-2027 SCION Consortium. All rights reserved.

where $I_j^{k,(r-1)}$ means that the value of I_j^k will be updated based on the value of $p_j^{(r-1)*}$ employing (5). The coefficients of step sizes are the subgradient values. It is also obvious that the derivatives of each multiplier are different which means that they are decoupled, so the update can be achieved through a parallel way actually.

All the sub-algorithms of the proposed algorithm JUBPA have been introduced. The proof of why algorithm of JUBPA can converge is as the following:

Theorem 2. *Algorithm 2 can converge and can achieve a local optimal solution.*

Proof. See Appendix 7.2

□

4.4 Algorithm Summary

DV-MOS2 consists of Markov approximation embedded with JUBPA, whose convergence can be guaranteed because the convergences of Markov approximation and JUBPA are given in [44] and theorem 2, respectively. The complexity of DV-MOS2 mainly comes from UA and BA. For UA stage, the worst case happens when J_r UE who proposed UA changing at round r have the exactly same preference list for the satellites. What's more, all the satellites can not accept UE anymore because of the constraints. As a result, the UE who proposed the requirement will be rejected by all the satellites. The complexity should be $|\mathcal{S}_z| \times J_r$. For BA stage, the worst case happens when the profile function values of all the UE-subcarrier pairs have the positive values. As a result, it should be updated for all the pairs in the profile which means the complexity is $K \times J_r/|\mathcal{S}_z|^2$. Here we assume that all the satellites get the same amount of UE to serve.

©2023-2027 SCION Consortium. All rights reserved.

5 Simulation Results

5.1 Simulation Environments and Settings

To evaluate the DV-MOS2 in a practical setting, we consider a ***Walker Constellation Design Pattern*** for a M-LEO satellite communication system. The constellation consists of 1000 satellites deployed at an altitude of 550 km with an orbital inclination angle of $70°$. The communication system operates at a carrier frequency of $f_c = 6$ GHz, with each subcarrier occupying a bandwidth of 10 MHz. A total of 25 UEs are uniformly distributed within a circular area of radius 1500 km, centered at $\boldsymbol{a}_{\text{UEC}}$. The coordinates of the satellites constellation and UE are shown in Fig. 5. Throughout the simulations, unless otherwise specified, we adopt the parameters reported in Table 3 (see [46] and references therein).

5.2 DV-MOS2 Approach Verification

5.2.1 DV-MOS2 Convergence Verification

In Fig.6(a), we observe that DV-MOS2, implemented via Algorithm1, exhibits consistent convergence behavior under different shadowing conditions ($SF = 1, 2,$ and 3dB). As expected, better channel quality (smaller shadowing factor) enables higher achievable sum rates, which is consistent with the trend also shown in Fig. 8. At the same time, the number of iterations required for convergence varies across fading levels. Under severe fading (e.g., $SF = 3$ dB), it becomes more challenging to identify satellite groups that jointly satisfy the system constraints and yield high data rates. Consequently, the algorithm stabilizes more quickly, leading to an earlier decay of the exploration probability. Conversely, under milder fading ($SF = 1$ dB), DV-MOS2 continues exploring larger candidate sets, resulting in higher final performance but requiring more iterations to converge. The presence of occasional drops even after the sum rate reaches high values. This behavior arises from the Markov approximation component of DV-MOS2, whose inherent exploration mechanism deliberately tests alternative satellite constellations in search of marginal performance gains before consolidating to a stable configuration. Fig. 6(b) further illustrates this behavior by showing the cumulative distribution function (CDF) of the achieved sum rates. The CDF curves confirm that smaller shadowing factors yield a clear rightward shift, indicating consistently higher rates across UEs. This validates not only the convergence of DV-MOS2 but also its robustness in adapting to different channel conditions.

5.2.2 Behavior of Matching Game-based UA and BA in DV-MOS2

Fig. 7 illustrates the convergence behavior of the matching-based UA and BA (Algorithm 3 and Algorithm 4) procedures when executed under a fixed PA policy, which can be derived from (25) by setting $r_{\min} = 3$ Mbps. The results confirm that the UA-BA combination converges reliably under different network sizes ($|\mathcal{U}| = 20$, 25, and 30). Notably, the sum rate improves markedly after the first iteration, but subsequent iterations yield additional gains. This is because, without invoking Algorithm 5, interference cannot be effectively managed, thereby limiting further performance improvement. Moreover, the sum rate grows with the number of UEs, since a larger user pool increases the likelihood of favorable satellite-user matches and more efficient bandwidth utilization.

©2023-2027 SCION Consortium. All rights reserved.

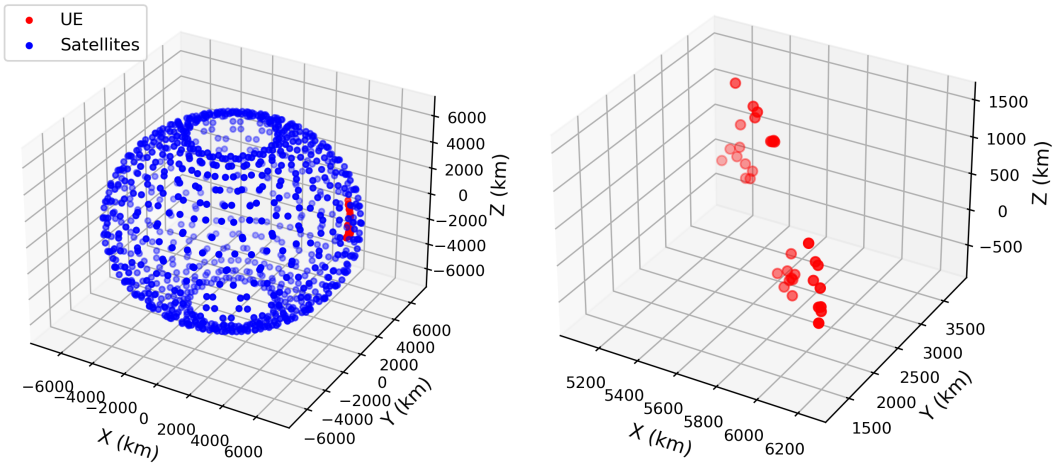


Figure 5: Spatial distributions of (a) satellites with UE and (b) UE.

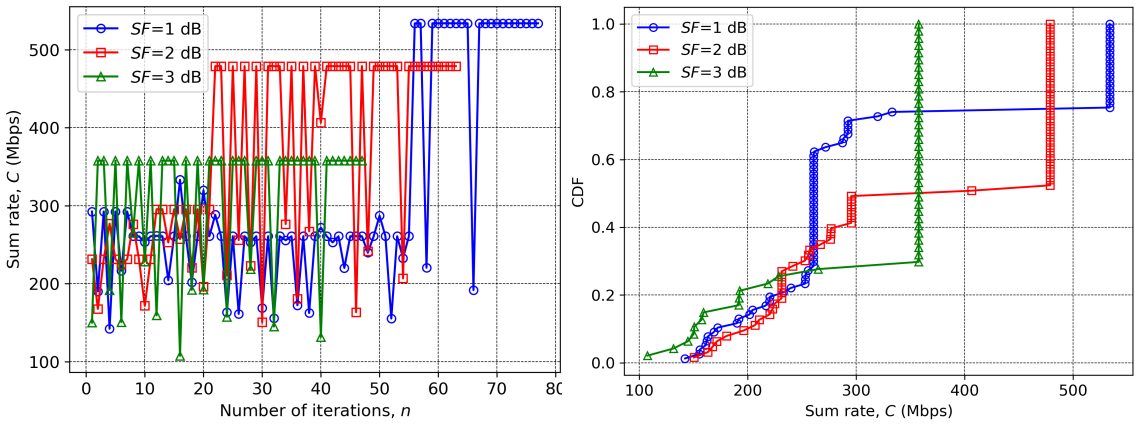
Table 3: General System Parameters

Parameters	**Value**
Number of satellites, $\lvert\mathcal{S}\rvert$	25×40
Number of UE, $\lvert\mathcal{U}\rvert$	30
Number of subcarriers, $\lvert\mathcal{B}\rvert$	25
Central frequency, f_c	6 GHz
Bandwidth, B	10 MHz
Orbits height, h_{sat}	550 km
Orbits inclined angle	70^o
Maximum power, P_{max}	5 W
Satellites amount, Z_{th}	10
Shadowing factor, SF	1 dB
Antenna gain, G_t	30 dB
Cone angle, φ (rad)	$5\pi/12$
UE area center, $\boldsymbol{a}_{\text{UEC}}$(km)	$[5765.39, 2717.12, 252.39]$

5.2.3 Effectiveness of JUBPA in DV-MOS2

Fig. 8 demonstrates the convergence behavior of the proposed JUBPA algorithm under different shadowing factors $SF = 1, 2, 3$ dB. The results confirm that JUBPA achieves stable convergence across all channel conditions. As expected, better channel quality, corresponding to smaller SF values, leads to higher achievable sum rates, since weaker shadowing implies less blockage and more reliable links. Moreover, JUBPA converges rapidly, typically within two to three iterations, which highlights its efficiency in practical implementations. Compared with the UA-BA combination, JUBPA yields a pronounced performance gain, underscoring the effectiveness of jointly incorporating PA into the matching-based UA and BA procedures.

©2023-2027 SCION Consortium. All rights reserved.



(a) (b)

Figure 6: DV-MOS2's sum rate (a) convergence and (b) CDF curve under different setup of SF values.

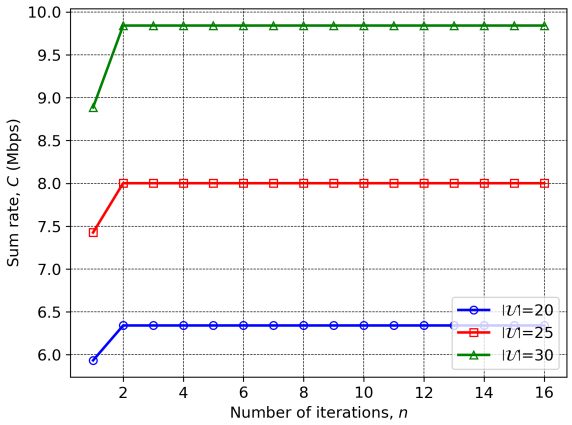


Figure 7: Convergence of matching game process under different network sizes.

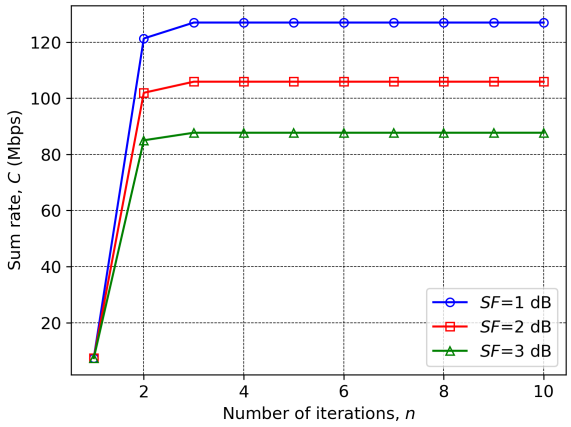


Figure 8: Convergence of JUBPA algorithm under different setup of SF values.

5.3 Performance Comparison

5.3.1 Gains of Joint UA-BA Matching in DV-MOS2

In order to verify the effectiveness of the matching game-based UA and BA components, we evaluate the performance of DV-MOS2 against the following two methods: (i) Fixed-UA + Fixed-BA: both UA and BA are predetermined in a static manner without employing matching game theory; (ii) Fixed-UA + Matching-BA: the UA is fixed, while the BA is optimized via the matching game algorithm (Algorithm 3 and Algorithm 4). These methods are tested under the same Markov approximation and PA procedures, ensuring a fair comparison that isolates the contribution of matching game-based UA and BA. The results are presented in Fig. 9, where the sum rate performance is plotted as a function of the cone angle φ, which varies from $\frac{\pi}{10}$ to $\frac{7\pi}{20}$ in steps of $\frac{\pi}{40}$. As expected, the achievable sum rate generally improves with larger φ, since a wider cone angle allows more satellites to be considered in the association and beam assignment process. However, the performance gaps among the three methods highlight the importance of applying matching game theory to both UA and BA. Specifically, the double matching scheme (DV-MOS2) consistently outperforms the baselines, demonstrating

©2023-2027 SCION Consortium. All rights reserved.

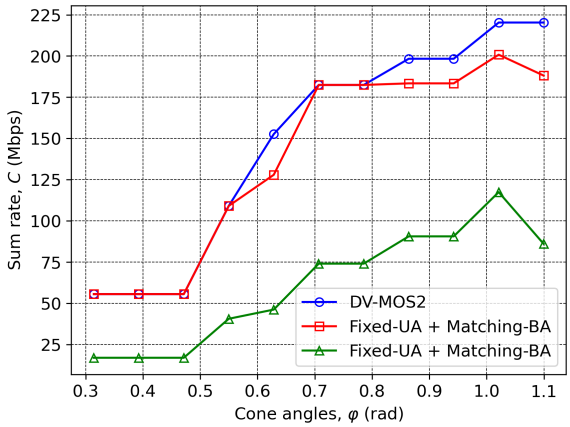


Figure 9: Sum rate comparison of different matching algorithms and different angle values.

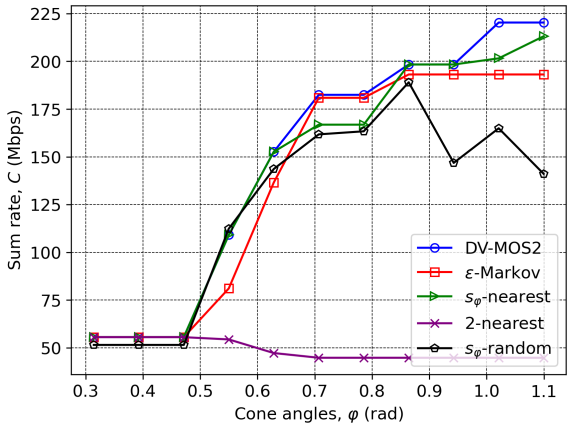


Figure 10: Sum rate comparison of different satellites selection algorithms.

the synergistic gain of jointly adapting both stages. In contrast, the Fixed-UA + Matching-BA method achieves moderate improvement over the fully fixed baseline, but its performance saturates when φ grows, as fixing UA limits the ability to exploit the enlarged candidate satellite set. Finally, the double fixed method exhibits the poorest performance and even suffers performance degradation at higher φ values, where interference becomes more severe and cannot be effectively mitigated without adaptive UA and BA.

5.3.2 Comparative evaluation of Satellite Selection Strategies under Dynamic Visibility

To further gain insight of DV-MOS2, we conduct comparative experiments that highlight its capability not only in adaptively selecting satellites, but also in dynamically determining the number of active satellites while coping with visibility variations and constellation size constraints. For this purpose, we select the following four schemes as the baseline.

- ϵ-Markov [47]: Follows the general framework of the proposed algorithm, but the execution of either the E-stage or the C-stage is determined in a stochastic manner.
- s_φ-nearest: Selects the s_φ satellites closet to the UE cluster center.
- 2-nearest: Always selects the two closest satellites to the UE cluster center.
- s_φ-random: Randomly selects s_φ satellites without considering their locations.

s_φ denotes the number of serving satellites adaptively determined by DV-MOS2 as a function of the cone angle φ. For a fair comparison, all methods (except the 2-nearest scheme) are assumed to select the same number of satellites, s_φ, as determined by DV-MOS2, while executing an identical JUBPA process. The 2-nearest method fixes the number of serving satellites to two, irrespective of the cone angle.

Fig. 10 presents the sum rate performance of the proposed DV-MOS2 framework in comparison with the above baselines under varying cone angles $\varphi \in \left[\frac{\pi}{10}, \frac{7\pi}{20}\right]$ for a network with $|\mathcal{U}| = 35$. From the results, we observe that DV-MOS2 consistently achieves the highest sum rate across the entire range of cone angles. In particular, the performance gap between DV-MOS2 and the 2-nearest scheme is remarkable. Since the 2-nearest scheme fixes the

©2023-2027 SCION Consortium. All rights reserved.

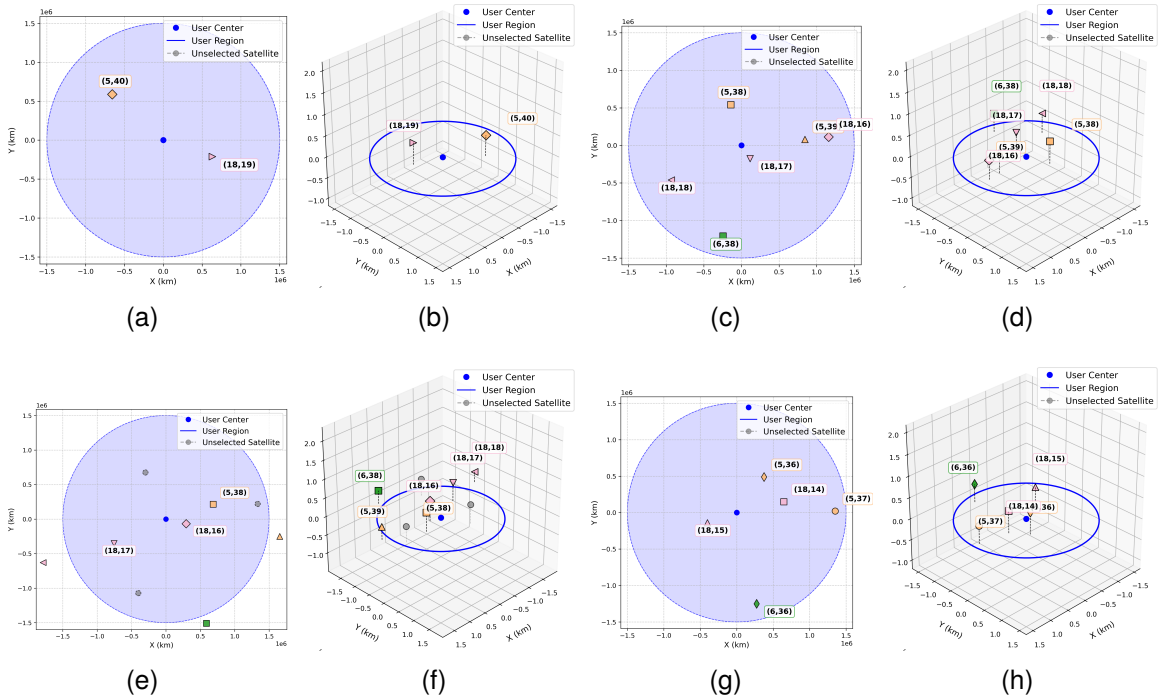


Figure 11: Visualized satellite trajectories: (a) 2D at $t = 1$, (b) 3D at $t = 1$, (c) 2D at $t = 7$, (d) 3D at $t = 7$, (e) 2D at $t = 9$, (f) 3D at $t = 9$, (g) 2D at $t = 15$, (h) 3D at $t = 15$.

number of serving satellites to two, it fails to exploit the potential spatial diversity provided by larger visibility regions when φ increases. By contrast, DV-MOS2 dynamically adapts the number of selected satellites, thereby striking a balance between interference mitigation and multi-satellite diversity. This adaptivity translates directly into substantial throughput gains. Moreover, while the s_φ-nearest and s_φ-random baselines partially reflect the constellation size constraint by fixing the number of selected satellites to s_φ, they neglect the coupled impact of cone-angle-shaped visibility and interference. As a result, their performance tends to plateau or even degrade at larger cone angles. By contrast, DV-MOS2 jointly incorporates constellation size and visibility geometry into the selection and allocation process, maintaining consistently superior performance across all cone-angle settings. In addition to the above observations, Fig. 10 shows that the ϵ-Markov method achieves competitive but inferior results compared to DV-MOS2, owing to its stochastic decision-making between exploration and consolidation, which prevents consistent exploitation of favorable satellite constellations. These results collectively demonstrate that the proposed DV-MOS2 framework is not only adaptive in the number of satellites but also better suited to address visibility constraints and constellation dynamics than all benchmark.

Finally, to evaluate the influence of the inherent dynamism of M-LEO, we simulated the time-varying selection results obtained by DV-MOS2. Fig. 11 illustrates the constellation snapshot of the chosen satellites under the proposed workflow, with simulation results recorded from $t = 1$ to $t = 19$ minutes at an interval of 2 minutes. First, the number of selected satellites varies continuously over time, which is a direct consequence of the dynamic evolution of the constellation and the resulting changes in satellite visibility. Second, as highlighted in Fig. 11(f) at $t = 9$ minutes, there exist three visible satellites above the service area that are not selected by DV-MOS2. According to the s_φ-nearest rule, they should have been chosen instead of satellites $s_{6,38}$ and $s_{18,18}$. This indicates that selecting the geographically closest

©2023-2027 SCION Consortium. All rights reserved.

satellites does not guarantee optimal performance, so underscoring the advantage of the proposed strategy.

5.3.3 Sensitivity analysis

Although a full parameter sweep (e.g., over f_c) is not included, the report already provides sensitivity results along two key dimensions that capture the main sources of variability in practical M-LEO operation. First, we vary the number of UEs $|\mathcal{U}|$ to reflect different traffic loads, and the proposed method maintains consistent performance advantages and stable convergence behavior across the tested user populations. Second, we vary the shadowing fading factor SF to represent diverse channel conditions, and the results show that the proposed DT-assisted selection and allocation remains robust under harsher propagation while preserving its gain over baselines. These two studies jointly serve as the sensitivity analysis requested, while extending the evaluation to additional physical-layer parameters such as carrier frequency f_c is left for future work.

©2023-2027 SCION Consortium. All rights reserved.

6 Conclusion and Future Work

In this report, we addressed the joint optimization of satellite selection, UA, BA, and PA in M-LEO constellations under dynamic visibility constraints. To tackle the inherent NP-hardness of the formulated problem, we proposed the DV-MOS2 framework, which integrates Markov approximation with a matching game-based approach for association and RA. Simulation results on the Walker constellation demonstrated that DV-MOS2 achieves stable convergence under various channel conditions and significantly outperforms four state-of-the-art baselines. In particular, the proposed algorithm provides, on average, a 7.85% sum-rate gain over the best-performing benchmark with affordable computational complexity. Moreover, dynamic simulations confirmed that the selected serving satellites adapt seamlessly to time-varying constellation visibility, thereby verifying the robustness and generality of the approach. An additional insight is that the commonly used closest-satellite selection rule does not necessarily yield the best performance, underscoring the necessity of adaptive and visibility-aware satellite selection in practical M-LEO systems.

In the future, several extensions follow naturally from the DT-assisted M-LEO optimization workflow presented in this deliverable. First, while DV-MOS2 currently targets sum-rate maximization under per-satellite power budgets and minimum-rate QoS, WP5 use cases motivate enriching the DT service layer with additional M2M-centric constraints such as latency bounds, reliability targets, and handover stability. Second, the present formulation assumes that the DT has timely access to satellite states/positions and can execute slot-wise decisions; a practical next step is to explicitly model DT synchronization and prediction errors and to develop robust variants of the Markov-selection and inner JUBPA loop that maintain feasibility and performance under such uncertainty. Third, the current study focuses on down link access within a fixed service region; extending the DT model to multi-region, multi-tenant operation and to integrated satellite-terrestrial coordination would better reflect end-to-end M2M service delivery in SCION. Finally, from an implementation perspective, the workflow can be modularized into DT software components, enabling real-time execution. Subsequent work will therefore focus on packaging these modules with clearly defined interfaces and profiling their complexity to support deployment-oriented DT control loops.

©2023-2027 SCION Consortium. All rights reserved.

7 Appendix

7.1 Proof of Theorem 1

According to the operation in Algorithm 3, the matching μ_{UA} can capture quantity $\sum_j PF_{o,i}^{\mathsf{UA}}(j)$ increasing after accommodating one UE, which means that $\sum_j PF_{o,i}^{\mathsf{UA}}(j)^{[r+1]} \geq \sum_j PF_{o,i}^{\mathsf{UA}}(j)^{[r]}$. It has been proved that $R(t)$ increases with $\sum_j PF_{o,i}^{\mathsf{UA}}(j)$ [45], $R(\boldsymbol{x}^{[r+1]}) \geq R(\boldsymbol{x}^{[r]})$. It is very obvious that μ_{BA} can also capture the increment of the network throughput given the UA result and transmitted power. It means that $R(\boldsymbol{y}^{[r+1]}; \boldsymbol{x}, \boldsymbol{z}, \boldsymbol{p}, t) \geq R(\boldsymbol{y}^{[r]}; \boldsymbol{x}, \boldsymbol{z}, \boldsymbol{p}, t)$. With the UA matching results, we have $R(\boldsymbol{x}^{[c_{\mathrm{o}}+1,c_{\mathrm{i}}]},\boldsymbol{y}^{[c_{\mathrm{o}}+1,c_{\mathrm{i}}]}; \boldsymbol{p}, t) \geq R(\boldsymbol{x}^{[c_{\mathrm{o}}+1,c_{\mathrm{i}}-1]},\boldsymbol{y}^{[c_{\mathrm{o}}+1,c_{\mathrm{i}}-1]}; \boldsymbol{p}, t)$.

7.2 Proof of Theorem 2

To prove the convergence of the proposed Algorithm 2, we just need to prove the monotonicity of each step.

$$\begin{aligned} R(\boldsymbol{x}^{[c_{\mathrm{o}}+1,c_{\mathrm{i}}]}, \boldsymbol{y}^{[c_{\mathrm{o}}+1,c_{\mathrm{i}}]}, \boldsymbol{p}^{[c_{\mathrm{o}}+1,c_{\mathrm{i}}]}) &\overset{(1)}{\geq} R(\boldsymbol{x}^{[c_{\mathrm{o}}+1,c_{\mathrm{i}}]}, \boldsymbol{y}^{[c_{\mathrm{o}}+1,c_{\mathrm{i}}]}, \boldsymbol{p}^{[c_{\mathrm{o}}+1,c_{\mathrm{i}}-1]}) \\ &\overset{(2)}{\geq} R(\boldsymbol{x}^{[c_{\mathrm{o}}+1,c_{\mathrm{i}}-1]}, \boldsymbol{y}^{[c_{\mathrm{o}}+1,c_{\mathrm{i}}-1]}, \boldsymbol{p}^{[c_{\mathrm{o}}+1,c_{\mathrm{i}}-1]}). \end{aligned} \tag{79}$$

(2) has been proved. (1) is because the the PA part is designed based on the gradient type of method so the non-decreasing monotonicity can be achieved with respect to $\boldsymbol{p}$.

©2023-2027 SCION Consortium. All rights reserved.

References

[1] P. Yang, Y. Xiao, M. Xiao, and S. Li, "6G wireless communications: Vision and potential techniques," *IEEE Network*, vol. 33, no. 4, pp. 70–75, 2019.

[2] C.-X. Wang, X. You, X. Gao, X. Zhu, Z. Li, C. Zhang, H. Wang, Y. Huang, Y. Chen, H. Haas, J. S. Thompson, E. G. Larsson, M. D. Renzo, W. Tong, P. Zhu, X. Shen, H. V. Poor, and L. Hanzo, "On the road to 6G: Visions, requirements, key technologies, and testbeds," *IEEE Communications Surveys & Tutorials*, vol. 25, no. 2, pp. 905–974, 2023.

[3] Z. Xiang, X. Gao, K.-X. Li, and X.-G. Xia, "Massive mimo downlink transmission for multiple LEO satellite communication," *IEEE Transactions on Communications*, vol. 72, no. 6, pp. 3352–3364, 2024.

[4] Z. Jia, C. Dong, K. Guo, and Q. Wu, "The potential of LEO satellites in 6G space-air-ground enabled access networks," 2023. [Online]. Available: https://arxiv.org/abs/2307.00234

[5] R. Deng, B. Di, H. Zhang, L. Kuang, and L. Song, "Ultra-dense LEO satellite constellations: How many LEO satellites do we need?" *IEEE Transactions on Wireless Communications*, vol. 20, no. 8, pp. 4843–4857, 2021.

[6] B. Lee, J.-H. Lee, and Y.-C. Ko, "Fairness-aware throughput optimization in low earth orbit satellite communication networks using a 3d spherical coordinate system," *IEEE Transactions on Wireless Communications*, vol. 23, no. 10, pp. 14 007–14 019, 2024.

[7] L. Zhao, C. Wang, K. Zhao, D. Tarchi, S. Wan, and N. Kumar, "Interlink: A digital twin-assisted storage strategy for satellite-terrestrial networks," *IEEE Transactions on Aerospace and Electronic Systems*, vol. 58, no. 5, pp. 3746–3759, 2022.

[8] J. Li, B. Liu, and M. Peng, "Joint beamforming design and satellite selection for integrated communication and navigation in LEO satellite networks," in *GLOBECOM 2024 - 2024 IEEE Global Communications Conference*, 2024, pp. 3273–3278.

[9] C. Dai, Y. Chen, B. Zang, L. Li, L. Zhang, K. Wang, and M. Wu, "A fast satellite selection algorithm based on nswoa for multi-constellation LEO satellite dynamic opportunistic navigation," *Applied Sciences*, vol. 15, no. 13, 2025. [Online]. Available: https://www.mdpi.com/2076-3417/15/13/7564

[10] Z. Li and B. Shang, "Enriched k-tier heterogeneous satellite networks model with user association policies," 2025. [Online]. Available: https://arxiv.org/abs/2505.09917

[11] Y. Hu, F. Qiu, F. Zheng, and J. Zhao, "Multi-dimensional resource allocation strategy for LEO satellite communication uplinks based on deep reinforcement learning," *Journal of Cloud Computing*, vol. 13, no. 1, p. 56, 2024.

[12] Y. Wu, G. Hu, F. Jin, and J. Zu, "A satellite handover strategy based on the potential game in LEO satellite networks," *IEEE Access*, vol. 7, pp. 133 641–133 652, 2019.

[13] S. Ni, J. Liu, M. Sheng, J. Li, and X. Zhao, "Joint optimization of user association and resource allocation in cache-enabled terrestrial-satellite integrating network," *Science China Information Sciences*, vol. 64, no. 8, p. 182306, 2021.

©2023-2027 SCION Consortium. All rights reserved.

[14] Y. Liu, C. Lu, and W. Xu, "Satellite access points selection for cell-free LEO networks," 2024, available at SSRN: https://ssrn.com/abstract=5327864.

[15] L. Wang, S. Liu, W. Wang, and Z. Fan, "Dynamic uplink transmission scheduling for satellite internet of things applications," *China Communications*, vol. 17, no. 10, pp. 241–248, 2020.

[16] L.-H. Shen, Y. Ho, K.-T. Feng, L.-L. Yang, S.-H. Wu, and J.-M. Wu, "Hierarchical multi-agent multi-armed bandit for resource allocation in multi-LEO satellite constellation networks," in *2023 IEEE 97th Vehicular Technology Conference (VTC2023-Spring)*, 2023, pp. 1–5.

[17] H. Nguyen-Kha, V. N. Ha, E. Lagunas, S. Chatzinotas, and J. Grotz, "LEO-to-user assignment and resource allocation for uplink transmit power minimization," in *WSA & SCC 2023; 26th International ITG Workshop on Smart Antennas and 13th Conference on Systems, Communications, and Coding*, 2023, pp. 1–6.

[18] ——, "Two-tier user association and resource allocation design for integrated satellite-terrestrial networks," in *2023 IEEE International Conference on Communications Workshops (ICC Workshops)*, 2023, pp. 1234–1239.

[19] Y. Guo, C. Skouroumounis, S. Chatzinotas, and I. Krikidis, "On user association in large-scale heterogeneous LEO satellite network," 2024. [Online]. Available: https://arxiv.org/abs/2405.06978

[20] M. Mahyoub, H. Yanikomeroglu, G. K. Kurt, and S. Martel, "Visibility-aware user association and resource allocation in multi-slice LEO satellite networks," *Authorea Preprints*, 2024.

[21] E. Kim, I. P. Roberts, T. Lee, and J. G. Andrews, "Satellite selection for in-band coexistence of dense LEO networks," 2025. [Online]. Available: https://arxiv.org/abs/2503.15262

[22] L. Yang, X. Yang, and Z. Bu, "A conditional handover strategy based on trajectory prediction for high-speed terminals in LEO satellite networks," in *2024 IEEE International Conference on Communications Workshops (ICC Workshops)*, 2024, pp. 1697–1701.

[23] Z. Hongtao, W. Zhenyong, L. Dezhi, Y. Mingchuan, and G. Qing, "Double grouping-based group handover scheme for mega LEO satellite networks," *China Communications*, vol. 22, no. 2, pp. 77–94, 2025.

[24] S. Zhang, A. Liu, and X. Liang, "A multi-objective satellite handover strategy based on entropy in LEO satellite communications," in *2020 IEEE 6th International Conference on Computer and Communications (ICCC)*, 2020, pp. 723–728.

[25] F. Wang, D. Jiang, Z. Wang, J. Chen, and T. Q. S. Quek, "Seamless handover in LEO based non-terrestrial networks: Service continuity and optimization," *IEEE Transactions on Communications*, vol. 71, no. 2, pp. 1008–1023, 2023.

[26] S. Zhang, L. Guo, W. Mu, J. Wang, and Y. Liu, "Multi-objective satellite selection strategy based on entropy," in *2021 13th International Conference on Wireless Communications and Signal Processing (WCSP)*, 2021, pp. 1–5.

©2023-2027 SCION Consortium. All rights reserved.

[27] M. Y. Abdelsadek, G. K. Kurt, and H. Yanikomeroglu, "Distributed massive mimo for LEO satellite networks," *IEEE Open Journal of the Communications Society*, vol. 3, pp. 2162–2177, 2022.

[28] J. Li, G. Sun, Q. Wu, D. Niyato, J. Kang, A. Jamalipour, and V. C. M. Leung, "Collaborative ground-space communications via evolutionary multi-objective deep reinforcement learning," *IEEE Journal on Selected Areas in Communications*, vol. 42, no. 12, pp. 3395–3411, 2024.

[29] Y. Wang, T. Ma, X. Qin, X. Zhang, Z. Zhang, and H. Zhou, "Satellite–aircraft handover in ultra-dense LEO satellite networks," *IEEE Transactions on Vehicular Technology*, vol. 74, no. 3, pp. 4946–4961, 2025.

[30] Y. Sun, J. Zhu, and M. Peng, "Beam management in low earth orbit satellite communication with handover frequency control and satellite-terrestrial spectrum sharing," 2024. [Online]. Available: https://arxiv.org/abs/2404.08967

[31] T. Leng, Y. Xu, G. Cui, and W. Wang, "Caching-aware intelligent handover strategy for LEO satellite networks," *Remote Sensing*, vol. 13, no. 11, 2021. [Online]. Available: https://www.mdpi.com/2072-4292/13/11/2230

[32] J. Zhu, Y. Sun, and M. Peng, "Beam management in low earth orbit satellite networks with random traffic arrival and time-varying topology," *IEEE Transactions on Vehicular Technology*, vol. 73, no. 9, pp. 13 352–13 367, 2024.

[33] I. Leyva-Mayorga, V. Gala, F. Chiariotti, and P. Popovski, "Continent-wide efficient and fair downlink resource allocation in LEO satellite constellations," in *ICC 2023 - IEEE International Conference on Communications*, 2023, pp. 6689–6694.

[34] Y. Zhou, R. Zhang, J. Liu, T. Huang, Q. Tang, and F. R. Yu, "A hierarchical digital twin network for satellite communication networks," *IEEE Communications Magazine*, vol. PP, no. 99, 2023.

[35] B. Mao, X. Zhou, J. Liu, and N. Kato, "Digital twin satellite networks towards 6G: Motivations, challenges, and future perspectives," *IEEE Network*, vol. PP, no. 99, 2023.

[36] Z. Ji, S. Wu, and C. Jiang, "Cooperative multi-agent deep reinforcement learning for computation offloading in digital twin satellite edge networks," *IEEE Journal on Selected Areas in Communications*, vol. 41, no. 11, pp. 3414–3429, 2023.

[37] H. Fan, J. Long, L. Liu, and Z. Yang, "Dynamic digital twin and online scheduling for contact window resources in satellite network," *IEEE Transactions on Industrial Informatics*, vol. 19, no. 5, pp. 7217–7227, 2023.

[38] L. Zhao, C. Wang, K. Zhao, D. Tarchi, S. Wan, and N. Kumar, "Interlink: A digital twin-assisted storage strategy for satellite-terrestrial networks," *IEEE Transactions on Aerospace and Electronic Systems*, vol. 58, no. 5, pp. 3746–3759, 2022.

[39] T. Q. Duong, L. D. Nguyen, T. T. Bui, K. D. Pham, and G. K. Karagiannidis, "Machine learning-aided real-time optimized multibeam for 6G integrated satellite-terrestrial networks: Global coverage for mobile services," *IEEE Network*, vol. 37, no. 2, pp. 86–93, 2023.

[40] H. Chen, M. Xiao, and Z. Pang, "Satellite-based computing networks with federated learning," *IEEE Wireless Communications*, vol. 29, no. 1, pp. 78–84, 2022.

©2023-2027 SCION Consortium. All rights reserved.

[41] Z. Lai, Y. Deng, H. Li, Q. Wu, and Q. Zhang, "Space digital twin for secure satellite internet: Vulnerabilities, methodologies and future directions," *IEEE Network*, vol. PP, no. 99, 2023.

[42] A. Fastenbauer, M. Kaneko, P. Svoboda, and M. Rupp, "Impact of elevation angle on multi-beam LEO satellite communication systems," *IEEE Access*, vol. 13, pp. 71 723–71 737, 2025.

[43] "Quasi deterministic radio channel generator (quadriga)," https://quadriga-channel-model.de/.

[44] M. Chen, S. C. Liew, Z. Shao, and C. Kai, "Markov approximation for combinatorial network optimization," *IEEE Transactions on Information Theory*, vol. 59, no. 10, pp. 6301–6327, 2013.

[45] T. LeAnh, N. H. Tran, W. Saad, L. B. Le, D. Niyato, T. M. Ho, and C. S. Hong, "Matching theory for distributed user association and resource allocation in cognitive femtocell networks," *IEEE Transactions on Vehicular Technology*, vol. 66, no. 9, pp. 8413–8428, 2017.

[46] A. Wong, R. Pogorzelski, D. Sullivan, and K. Bhasin, "Nasa small satellite communication link analysis and performance," in *33rd Annual AIAA/USU Conference on Small Satellites*, 2019, pp. SSC19–VIII–05.

[47] Q. Zhu and J. Zheng, "A V2V task offloading decision algorithm for multi-rat vehicular networks," in *GLOBECOM 2024 - 2024 IEEE Global Communications Conference*, 2024, pp. 740–745.

©2023-2027 SCION Consortium. All rights reserved.